molecules

MDPI

Article

Trifluoromethoxy- and Fluorobenzhydryl-Tuned Nickel Catalysts for Polyethylene Elastomers

Ming Liu [1], Min Sun [1], Yanping Ma [2,*], Yizhou Wang [2], Mingfeng Li [1,*] and Wen-Hua Sun [2,*]

[1] State Key Laboratory of Petroleum Molecular & Process Engineering, SINOPEC Research Institute of Petroleum Processing Co., Ltd., Beijing 100083, China; liuming.ripp@sinopec.com (M.L.); sunmin.ripp@sinopec.com (M.S.)

[2] Key Laboratory of Engineering Plastics, Beijing National Laboratory for Molecular Sciences, Institute of Chemistry Chinese Academy of Sciences, Beijing 100190, China; wangyizhou13@iccas.ac.cn

* Correspondence: myanping@iccas.ac.cn (Y.M.); limf.ripp@sinopec.com (M.L.); whsun@iccas.ac.cn (W.-H.S.)

Abstract

A series of *para*-trifluoromethoxy-substituted and fluorobenzhydryl-functionalized 1,2-bis(imine)acenaphthene ligands: 1-[2,6-{(4-F-C_6H_4)$_2$CH}$_2$-4-$F_3COC_6H_2$N]-2-(ArN)$C_2C_{10}H_6$ (Ar = 2,6-$Me_2C_6H_3$ **L1**, 2,6-$Et_2C_6H_3$ **L2**, 2,6-i$Pr_2C_6H_3$ **L3**, 2,4,6-$Me_3C_6H_2$ **L4**, 2,6-Et_2-4-MeC_6H_2 **L5**), were synthesized and used to generate their corresponding nickel(II) bromide complexes (**Ni1**–**Ni5**). Elemental analysis, ^{19}F NMR, and FT-IR spectroscopy were employed to characterize these five nickel complexes. Single-crystal X-ray diffraction of **Ni2** and **Ni4** confirmed distorted tetrahedral geometries. Upon activation with either $EtAlCl_2$ (ethylaluminum dichloride) or EASC (ethyl aluminum sesquichloride), these complexes showed exceptional high activities (up to 22.0 × 10^6 g PE mol^{-1} (Ni) h^{-1}) and remarkable thermal stability (4.82 × 10^6 g PE mol^{-1}(Ni) h^{-1} at 80 °C) towards ethylene polymerization. The resulting polyethylenes are highly branched, with the type and extent of branches tunable by temperature, solvent, and co-catalyst choice. Moreover, these polymers demonstrated excellent tensile strength (σ_b up to 20.7 MPa) and elastic recovery (up to 58%), characteristic of thermoplastic elastomers (TPEs). These results highlight the dual role of trifluoromethoxy and fluorobenzhydryl groups in enhancing catalytic performance and polymer properties.

Keywords: nickel catalysts; dual steric-electronic tuning; highly branched polyethylenes; high-temperature polymerization; thermoplastic elastomers (TPEs)

check for updates

Academic Editors: Michal Szostak and Angelo Nacci

Received: 17 May 2025
Revised: 4 June 2025
Accepted: 18 June 2025
Published: 23 June 2025

Citation: Liu, M.; Sun, M.; Ma, Y.; Wang, Y.; Li, M.; Sun, W.-H. Trifluoromethoxy- and Fluorobenzhydryl-Tuned Nickel Catalysts for Polyethylene Elastomers. *Molecules* **2025**, *30*, 2706. https://doi.org/10.3390/molecules30132706

Copyright: © 2025 by the authors. Licensee MDPI, Basel, Switzerland. This article is an open access article distributed under the terms and conditions of the Creative Commons Attribution (CC BY) license (https://creativecommons.org/licenses/by/4.0/).

1. Introduction

Thermoplastic olefin elastomers (TPEs) have emerged as indispensable polymeric materials due to their excellent mechanical properties, weather resistance, and processability. Their inherent compatibility with polyolefins and cost-effectiveness in enhancing low-temperature toughness have driven widespread applications across automotive, construction, footwear, and consumer goods [1–3]. Conventionally synthesized through ethylene/α-olefin copolymerization (e.g., 1-butene, 1-hexene), TPE production relies on advanced catalytic technologies such as Dow Chemical (Midland, MI, USA) Insite™ solution polymerization [4], ExxonMobil's Exxpol [5,6], and SABIC SK (Ulsan, South Korea) Nexlene™ processes [5]. However, the pursuit of more efficient catalytic systems capable of precise polymer architecture control remains a critical challenge in polyolefin chemistry.

A pivotal breakthrough occurred in the 1990s when Brookhart et al. discovered that α-diimine Ni/Pd complexes could serve as single-center catalysts for the homopoly-

merization of ethylene, generating branched polyethylene (PE) [7,8] via a chain-walking mechanism [9–12]. While this innovation sparked intensive research into late-transition metal catalysts [13–24], practical implementation was hindered by inherent limitations: insufficient thermal stability and low activity at industrially relevant temperatures. Recent advancements in iron-based α-olefin polymerization catalysts [25] have revitalized interest in addressing these challenges through innovative ligand design.

The catalytic performance of α-diimine nickel (II) complexes (**A**, Chart 1) is profoundly governed by structural modifications to the ligand framework, particularly through adjustments to the backbone geometry and *N*-aryl substituents. Strategic incorporation of bulky groups (such as benzhydryl and its derivatives, or cycloalkyl groups) [26–32] and para-substituents possessing varied electronic characteristics (-Me, -*t*Bu, -OMe, -Cl, -F, -NO_2) enables precise modulation of both steric protection and electronic environment at the metal center. Bulky substituents can effectively improve the thermal stability of catalysts by suppressing deactivation pathways at higher temperature [28,29,33,34], while these *para*-substituents influence the activities of catalysts by influencing the electron density of the metal center.

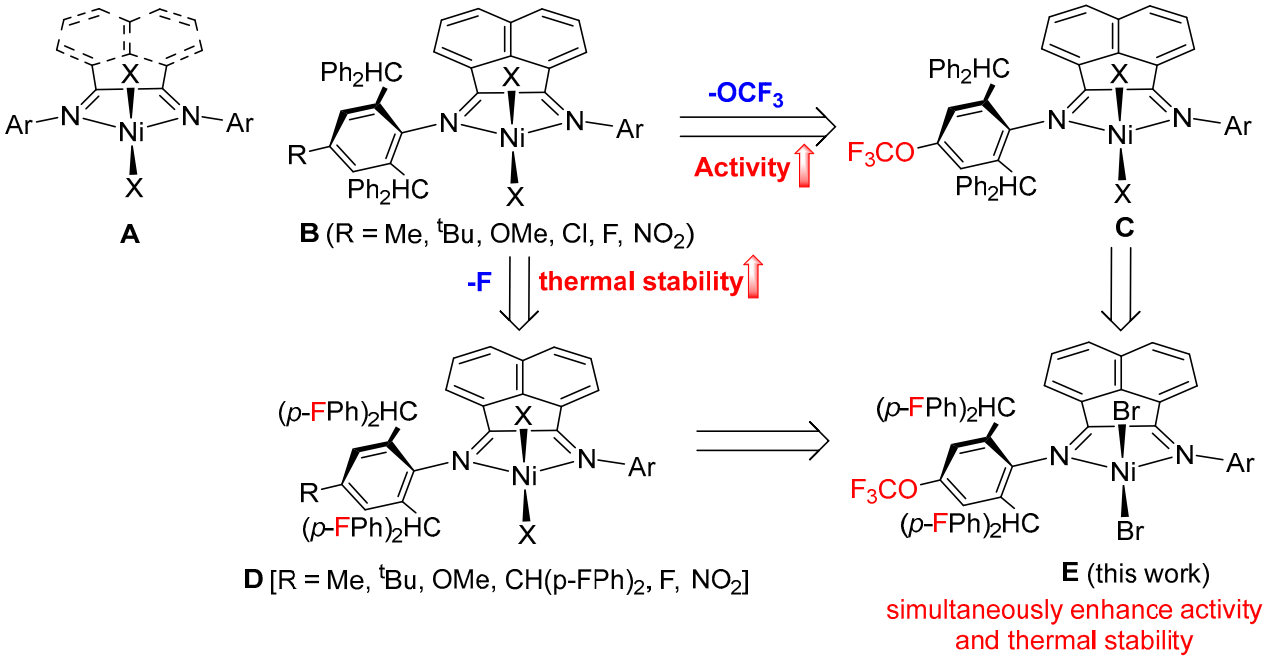


Chart 1. Structural evolution of *N*,*N*′-diiminoacenaphthene-nickel(II) halide precatalysts (**A**–**E**).

For instance, our group demonstrated that 2,6-benzhydryl-substituted asymmetric α-diimine-nickel(II) complexes (**B**, Chart 1) generate high-molecular-weight, branched PE with activities correlating to the substituent electronic effects (Me, *t*-Bu, OMe, Cl, F, NO_2) [35–38] at the *para*-positions of the *N*-aryl. Notably, catalysts bearing electron-withdrawing substituents tend to exhibit higher activity. When we introduced the strongly electron-withdrawing -OCF_3 group into the catalyst framework (**C**, Chart 1), the net positive charge at the nickel center was increased, boosting its activity up to 15.1 × 10^6 g PE mol^{-1} (Ni) h^{-1}. Remarkably, replacing conventional toluene with n-hexane as the reaction solvent further enhanced both catalytic performance and thermal stability [39].

Fluorine substitution has emerged as a powerful strategy for improving catalytic performance. Incorporating distal fluorine atoms into benzhydryl group (**D**, Chart 1) (Me [40], *t*-Bu [41], OMe [42], CH(*p*-FPh_2) [43], F [44], NO_2 [45]) markedly improved the thermal stability relative to non-fluorinated analogs (**B**, Chart 1). For example, $\mathbf{D_{NO2}}$, containing strong electron-withdrawing nitro and fluorine substituents, exhibited superior catalytic

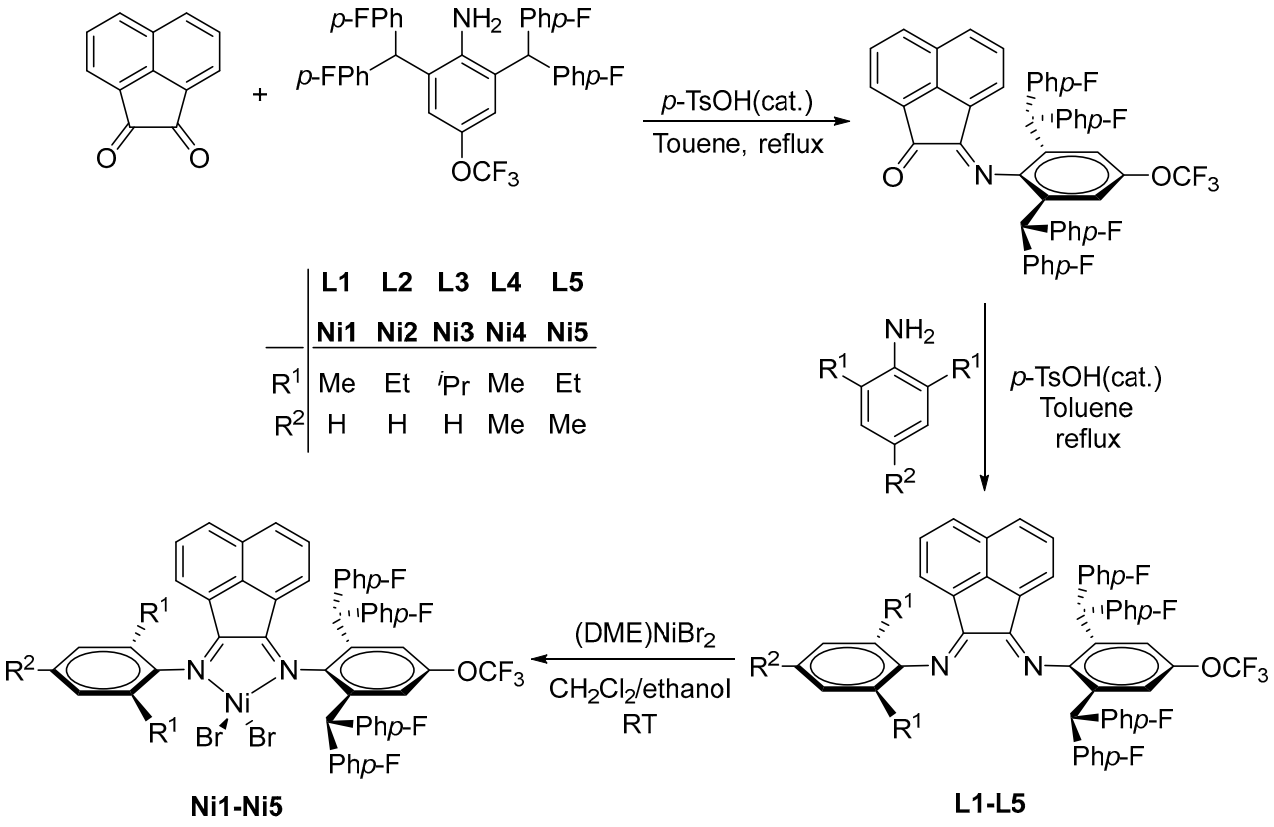
activity and thermal stability compared to $\mathbf{B_{NO2}}$ complex [38,45]. The $\mathbf{D_{tBu}}$/EASC catalytic system maintained high catalytic activity at 90 °C, and the resulting highly branched PE exhibited typical thermoplastic elastomer (TPE) characteristics [41].

Building on these insights, to synergistically boost both catalytic activity and thermal stability, we devised a dual-functional modification strategy herein: simultaneous installation of a strongly electron-withdrawing trifluoromethoxy group at the *N*-aryl *para*-position and distal fluorine atoms into the benzhydryl groups (**E**, Chart 1). The impact of these modifications on ethylene polymerization were systematically explored by exploring variables such as the ligand structure, co-catalyst choice, solvent (toluene vs. n-hexane), polymerization temperature, running time, and ethylene pressure. Exceptional performance was disclosed at industrially relevant temperatures (up to 80 °C), producing highly branched PE with tunable architectures. Comprehensive characterization (^{1}H/^{13}C/^{19}F NMR, FT-IR, GPC, DSC, XRD, etc.) was used to confirm structures of the ligands, complexes, and PE.

2. Results and Discussion

2.1. Synthesis and Characterization of the Ligands and Complexes

The *N*,*N*′-diimineacenaphthenes **L1**–**L5** 1-[2,6-{(4-FC_6H_4)$_2$CH}$_2$-4-$F_3COC_6H_2$N]-2-(ArN)$C_2C_{10}H_6$ (Ar = 2,6-$Me_2C_6H_3$ (**L1**), 2,6-$Et_2C_6H_3$ (**L2**), 2,6-i$Pr_2C_6H_3$ (**L3**), 2,4,6-$Me_3C_6H_2$ (**L4**), 2,6-Et_2-4-MeC_6H_2 (**L5**)), were prepared via a two-step process (Scheme 1).



Scheme 1. Synthesis of **L1**–**L5** and their corresponding nickel(II) bromide complexes **Ni1**–**Ni5**.

Firstly, 2-[2,6-bis(4,4′-difluorobenzhydryl)-4-(trifluoromethoxy)phenylimino]-acenaphthylen-1-one, was synthesized in reasonable yield by the acid catalyzed condensation reaction of acenaphthylene-1,2-dione with one molar equivalent of 2,6-bis(4,4′-difluorobenzhydryl)-4-(trifluoromethoxy)aniline [40–45]. This imine-ketone then reacted with the corresponding aniline to afford **L1**–**L5** in moderate yield (22.5–38.0%) (Scheme 1). All ligands were characterized by ^{1}H/^{13}C/^{19}F NMR (Figures S1–S15), FT-IR spectroscopy, and elemental

analysis, confirming their structural integrity. Nickel(II) bromide complexes **Ni1**–**Ni5** were generated in good yields (85–92%) by treatment of **L1**–**L5** with (DME)$NiBr_2$ (DME = 1,2-dimethoxyethane) in a mixed solvent system composed of dichloromethane and ethanol at room temperature (Scheme 1). All five complexes were characterized by elemental analysis, FT-IR and $^1H/^{19}F$ NMR spectroscopy (Figures S16–S25). Moreover, the molecular structures of **Ni2** and **Ni4** were confirmed by single-crystal X-ray diffraction analysis (see Table S1: Crystal data and structure refinement for **Ni2** and **Ni4**).

Single crystals of **Ni2** and **Ni4** of suitable quality for the X-ray determinations were grown by layering diethyl ether into their dichloromethane solutions at ambient temperature. The molecular structures of **Ni2** and **Ni4** (Figure 1) revealed distorted tetrahedral geometries with the nickel center coordinated by two bromide ligands and the two nitrogen donors from the *N*,*N*′-chelating bis(imine)acenaphthene, as is similar to those reported previously [40,44].

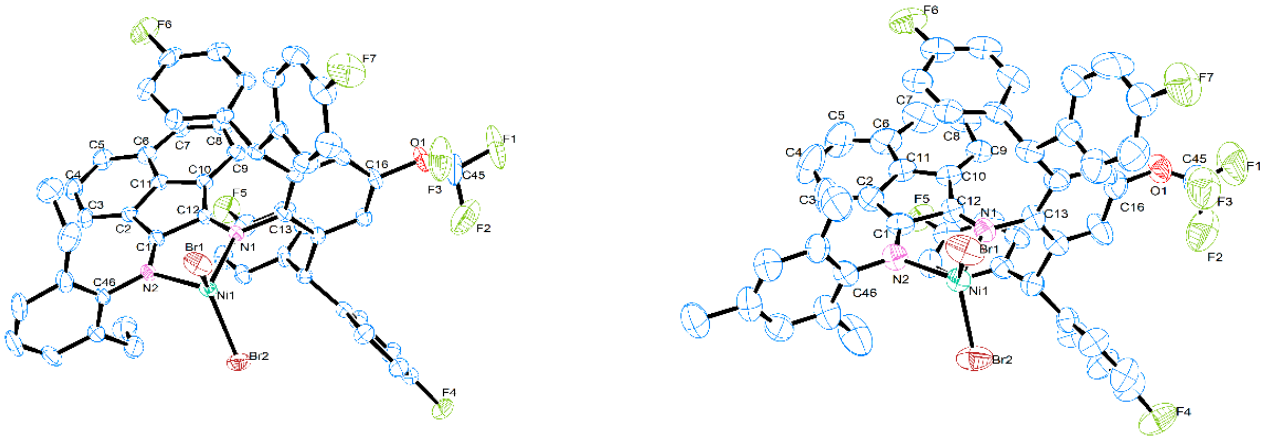


Figure 1. ORTEP diagram of **Ni2** (**a**) and **Ni4** (**b**) with the thermal ellipsoids shown at the 50% probability level. All hydrogen atoms have been omitted for clarity.

Key bond parameters including bond lengths and angles were listed in Table 1. The N1-Ni1-N2 bite angle of 82.73(12)° in **Ni2** is close to 82.6(3)° in **Ni4**, as is the same for Br1-Ni-Br2 bite angles (126.05(3)° (**Ni2**) vs. 126.56(7)° (**Ni4**)). Nickel-nitrogen bond lengths of Ni1–N1 [2.037(3) Å (**Ni2**), 2.041(7) Å (**Ni4**)] are slightly longer than those of Ni1-N2 [2.022(3) Å (**Ni2**), 2.011(7) Å (**Ni4**)], reflecting subtle steric variations between the aryl substituents. The $C{=}N_{imine}$ bond lengths for both complexes range from 1.261(11) to 1.290(4) Å, which are typical for this functional group [24]. Each imine unit is positioned nearly co-planar with the adjacent acenaphthene unit. The plane of the *N*-aryl group linked to N1 is almost perpendicular to the acenaphthene plane, with dihedral angles of 89.37° for **Ni2** and 89.04° for **Ni4**. On the other hand, due to the smaller steric hindrance, axial rotation is easier for the second *N*-aryl group (aryl = 2,6-$Et_2C_6H_3$ **Ni2**; 2,4,6-$Me_3C_6H_2$ **Ni4**), showing some variation [87.09° for **Ni2**, 87.41° for **Ni4**]. Notably, the F_3C–O bond has double bond character with distance values of 1.342(6) Å for **Ni2**, 1.23(5) Å for **Ni4**, suggesting partial ionic resonance contribution from the limiting form $ArO^+{=}CF^2F^-$ [46]. Meanwhile, there are no significant intermolecular contacts.

^{19}F NMR spectra of **L1**–**L5** (Figure S11–S15) and **Ni1**–**Ni5** (Figure S21–S25) corroborate ligand coordination. Taking **Ni1** as an example, the spectra were compared with that of the free ligand **L1**. For **L1**, two distinct signals at δ −116.12 and −116.35 arise from restricted rotation of the ortho-aryl groups leading to inequivalent $CH(4\text{-}FC_6H_4)_a(4\text{-}FC_6H_4)_b$ groups. Upon complexation (**Ni1**), these signals split further (δ −115.73 and −116.07), consistent

with previous studies [41]. The para-trifluoromethoxy resonance shifts upfield slightly from δ −58 in **L1** to δ −57 in **Ni1**, reflecting electronic modulation at the nickel center [39]. FT-IR spectra confirm effective coordination of the two imine nitrogen atoms to the nickel center via redshifted $\nu_{C=N}$ absorptions (ligands: 1672–1635 cm^{-1}; complexes: 1649–1618 cm^{-1}).

Table 1. Key bond parameters for **Ni2** and **Ni4**.

	Ni2	**Ni4**
Bond lengths (Å)		
Ni(1)-Br(1)	2.3342 (6)	2.3253 (16)
Ni(1)-Br(2)	2.3300 (7)	2.3388 (17)
Ni(1)-N(1)	2.037 (3)	2.041 (7)
Ni(1)-N(2)	2.022 (3)	2.011 (7)
N(1)-C(12)	1.290 (4)	1.261 (11)
N(1)-C(13)	1.446 (4)	1.448 (10)
N(2)-C(1)	1.283 (5)	1.289 (11)
N(2)-C(46)	1.440 (4)	1.450 (11)
$O(1)-C(45)_{CF3}$	1.342 (6)	1.23 (5)
Bond angles (°)		
N(1)-Ni(1)-N(2)	82.73 (12)	82.6 (3)
Br(1)-Ni(1)-Br(2)	126.05 (3)	126.56 (7)
N(1)-Ni(1)-Br(1)	110.13 (7)	109.70 (19)
N(1)-Ni(1)-Br(2)	110.20 (7)	111.2 (2)
N(2)-Ni(1)-Br(1)	110.18 (8)	107.7 (2)
N(2)-Ni(1)-Br(2)	109.08 (8)	110.3 (2)
C(45)-O(1)-C(16)	116.3 (4)	125 (3)

2.2. Ethylene Polymerization

2.2.1. Co-Catalyst Screening with **Ni1** for Ethylene Polymerization

The nickel-based catalyst precursor **Ni1** was evaluated in ethylene polymerization using five alkylaluminum reagents co-catalysts: methylaluminoxane (MAO), modified methylaluminoxane (MMAO), ethylaluminum dichloride ($EtAlCl_2$), ethylaluminum sesquichloride (EASC), and diethylaluminum chloride (Et_2AlCl)]. Polymerizations were conducted in toluene with ethylene pressure of 10 atm at 30 °C for 30 min, with the results summarized in Table 2.

Table 2. Ethylene polymerization results with **Ni1** using various alkylalumimum co-catalysts [a].

Run	**Co-Catalyst**	**Al/Ni**	**PE (g)**	**Activity** [b]	$\mathbf{M_w}$ [c]	$\mathbf{M_w/M_n}$ [c]	$\mathbf{T_m}$ [d] (°C)
1	MAO	2000	3.36	6.72	4.51	3.09	81.7
2	MMAO	2000	4.34	8.68	6.85	3.52	97.0
3	$EtAlCl_2$	300	6.59	13.2	5.96	3.49	66.4
4	EASC	300	4.39	8.78	7.54	2.48	99.6
5	Et_2AlCl	300	3.64	7.28	5.80	4.03	80.9

[a] Conditions: 1.0 μmol **Ni1**, 100 mL of toluene, 10 atm C_2H_4, 30 °C, 30 min; [b] 10^6 g (PE) mol^{-1} (Ni) h^{-1}; [c] M_w: $\times 10^5$ g mol^{-1}, M_w and M_w/M_n determined by GPC; [d] Determined by DSC.

All alkylaluminum-activated **Ni1** catalysts exhibited high ethylene polymerization activity, producing PEs with high molecular weight (~10^5 g mol^{-1}) and low melting temperatures (T_m < 100 °C) indicative of a branched polymer microstructure. The molecular weight distributions were unimodal in the range of 2.48–4.03, indicating single site active species. With regard to the three chloroalkylaluminums, $EtAlCl_2$ exhibits the highest activity, presumably attributed to its stronger Lewis acidity, enabling more efficient activation of

the metal center [47]. This phenomenon is contrasts to previously reported findings [48]. Among these co-catalysts screened, $EtAlCl_2$ and EASC exhibited the highest catalytic activities, reaching 13.2 × 10^6 g PE mol^{-1} (Ni) h^{-1} and 8.78 × 10^6 g PE mol^{-1} (Ni) h^{-1}, respectively. These values represent an enhancement compared to MAO and MMAO under identical conditions. Due to their superior performance, $EtAlCl_2$ and EASC were selected for subsequent optimization of polymerization conditions (such as Al/Ni ratio, polymerization temperature, reaction time, and ethylene pressure) and evaluation with other catalyst precursors.

2.2.2. Optimizing Ethylene Polymerization Parameters Using **Ni1**–**Ni5**/$EtAlCl_2$

In this section, we systematically investigated the effects of Al:Ni molar ratio, polymerization temperature, reaction time, ethylene pressure, and ligand structure on ethylene polymerization using **Ni1**–**Ni5** precatalysts activated by $EtAlCl_2$ (Table 3).

Table 3. Ethylene polymerization with **Ni1**–**Ni5**/$EtAlCl_2$ [a].

Run	Precat.	Al/Ni	T (°C)	T (min)	PE (g)	Activity [b]	M_w [c]	M_w/M_n [c]	T_m [d] (°C)
1	**Ni1**	300	30	30	6.59	13.2	5.96	3.49	66.4
2	**Ni1**	300	40	30	7.11	14.2	4.78	3.55	61.6
3	**Ni1**	300	50	30	4.77	9.54	4.26	2.70	45.5
4	**Ni1**	300	60	30	3.84	7.68	3.21	1.73	36.8
5	**Ni1**	300	70	30	2.42	4.84	2.64	2.51	35.8
6	**Ni1**	300	80	30	1.38	2.76	2.26	2.78	16.8
7	**Ni1**	100	40	30	5.37	10.7	4.18	2.61	58.6
8	**Ni1**	150	40	30	6.30	12.6	4.43	2.74	66.5
9	**Ni1**	200	40	30	8.59	17.2	4.59	2.29	59.4
10	**Ni1**	250	40	30	8.07	16.1	4.88	3.23	54.2
11	**Ni1**	200	40	5	1.63	19.6	2.78	3.00	62.3
12	**Ni1**	200	40	15	4.57	18.3	3.68	3.08	67.3
13	**Ni1**	200	40	45	10.6	14.1	4.86	2.16	56.3
14	**Ni1**	200	40	60	11.8	11.8	5.08	2.88	62.8
15 [e]	**Ni1**	200	40	30	3.58	7.16	3.73	2.59	55.4
16 [f]	**Ni1**	200	40	30	0.74	1.48	2.33	1.75	- [g]
17	**Ni2**	200	40	30	5.16	10.3	4.21	2.70	59.0
18	**Ni3**	200	40	30	3.37	6.74	6.68	2.90	51.1
19	**Ni4**	200	40	30	7.63	15.3	4.23	3.07	63.8
20	**Ni5**	200	40	30	6.98	14.0	3.57	2.22	58.7

[a] Conditions: 1.0 μmol pre-catalyst, 100 mL of toluene, 10 atm C_2H_4; [b] 10^6 g (PE) mol^{-1} (Ni) h^{-1}; [c] M_w: $\times 10^5$ g mol^{-1}, M_w and M_w/M_n determined by GPC; [d] Determined by DSC; [e] 5 atm C_2H_4; [f] 1 atm C_2H_4; [g] Broad and weak endotherms, amorphous polymers.

First, we systematically evaluated the polymerization behavior across reaction temperatures ranging from 30 °C to 80 °C, under fixed conditions: 10 atm ethylene pressure, Al/Ni = 300, 30 min (runs 1–6, Table 3). The results revealed that catalytic activity reached its peak at 40 °C (14.2 × 10^6 g PE mol^{-1} (Ni) h^{-1}), followed by a decrease at higher temperatures attributed to partial deactivation of active species and reduced ethylene solubility [49,50]. Despite this, the activity value of 2.76 × 10^6 g PE mol^{-1} (Ni) h^{-1} at 80 °C remained notably high, underscoring the positive influence of bulky substituents and the distal F group on thermal stability [39–41]. Concurrently, the polymer molecular weight gradually decreased from 5.96 × 10^5 g mol^{-1} to 2.26 × 10^5 g mol^{-1} with increasing the temperature from 30 to 80 °C, due to accelerated chain transfer rate [45,51–53]. Notably, over this temperature span, all polymers displayed narrow dispersity (M_w/M_n range: 1.73–3.55) and a unimodal distribution (Figure S26), confirming a single active species participated in the polymerization process. The polymer's melting point (T_m) inversely correlated with

the reaction temperature, likely due to reduced molecular weight and increased branching density at elevated temperatures, leading to reduced crystallinity. These results suggest that the high temperatures promote chain walking isomerization, enhancing branching [54].

Next, we fixed the polymerization temperature at 40°C and varied the Al:Ni molar ratio from 100:1 to 300:1 to assess the influence of co-catalyst concentration (runs 2, 7–10, Table 3). As the Al:Ni molar ratio increased, catalytic activity initially rose, reaching a peak of 17.2 × 10^6 g PE mol^{-1} (Ni) h^{-1} at 200:1. Beyond this optical ratio, the activity declined, indicating that excess $EtAlCl_2$ concentration may facilitate chain transfer from the Ni center to the Al center, resulting in chain termination [55].

Further analysis of reaction time dependence (runs 2, 11–14, Table 3) revealed a distinct inverse relationship between time and activity. The highest activity was achieved within the first 5 min (33.2 × 10^6 g PE mol^{-1} (Ni) h^{-1}), followed by a gradual decline, suggesting rapid initial activation of the Ni center by $EtAlCl_2$, and progressive deactivation of active species over time [41]. Nonetheless, catalytic activity remained robust at 60 min [11.8 × 10^6 g PE mol^{-1} (Ni) h^{-1}], highlighting the stability of the residual active species and their prolonged catalytic lifetime. Meanwhile, the PE molecular weight increased steadily from 2.78 × 10^5 g mol^{-1} to 5.08 × 10^5 g mol^{-1}, indicating that although some active sites deactivated, others retained activity, enabling continued chain growth over time. When polymerization pressures were lowered (10 atm, 5 atm, 1 atm), both catalytic activity and polymer molecular weight were found to diminish, likely due to the reduced ethylene concentration at lower pressure [38,44].

Under optimized conditions (Al/Ni = 200, 40 °C, 30 min, 10 atm), ligand modifications in **Ni1**–**Ni5** significantly impacted catalytic performance. All complexes exhibited high ethylene polymerization catalytic activity [6.74–17.2 × 10^6 g PE mol^{-1} (Ni) h^{-1}], producing high molecular weight PE (M_w: 3.57–6.68 × 10^5 g mol^{-1}) with low melting points (T_m: 51.1–63.8 °C), indicating a high degree of branching. The catalytic activity followed the order: **Ni1** > **Ni4** > **Ni5** > **Ni2** > **Ni3**, indicating that catalytic systems with smaller substituents demonstrate superior activity, by minimizing steric hindrance to ethylene coordination and insertion at the active site [45]. Conversely, **Ni3** bearing bulkier substituents, exhibited the lowest activity by yield the PE with highest molecular weight (6.68 × 10^5 g mol^{-1}, run 18, Table 3), suggesting that bulky substituents protect active species and mitigate chain termination.

2.2.3. Optimizing Ethylene Polymerization Parameters Using **Ni1**–**Ni5**/EASC

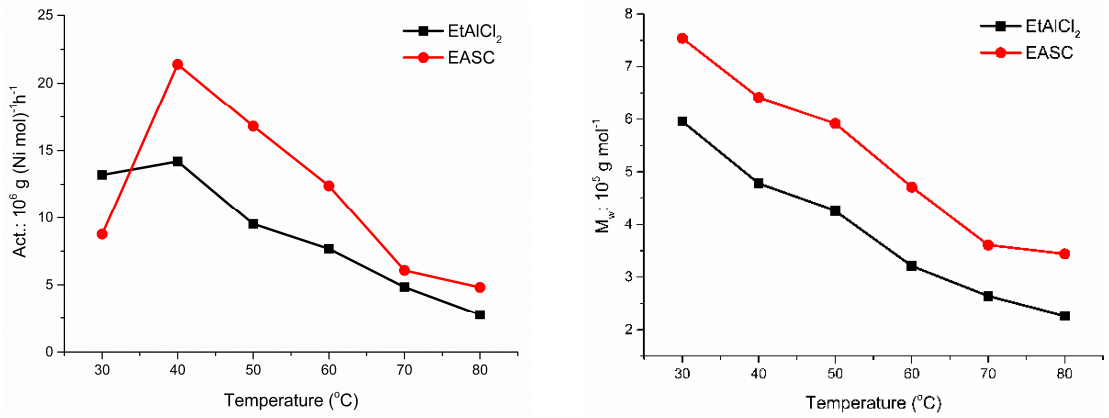
Similarly, we evaluated ethylene polymerization performance of **Ni1**–**Ni5** complexes using EASC as the co-catalyst, with experimental results listed in Table 4. The **Ni1**–**Ni5**/EASC system also exhibited efficient catalytic activity, yielding high molecular weight PE with narrow distribution and low melting points, indicative of branched polymer microstructures.

As the temperature rises from 30 °C to 80 °C (run 1–6, Table 4), the catalytic activity of **Ni1**/EASC initially increases to a maximum of 21.4 × 10^6 g PE mol^{-1}(Ni) h^{-1} at 40 °C, followed by a gradual decline, while polymer molecular weight steadily decreased—a pattern mirroring the **Ni1**/$EtAlCl_2$ system (Figure 2). Notably, **Ni1**/EASC showed 1.5-fold higher peak activity than **Ni1**/$EtAlCl_2$ [21.4 vs. 14.2 × 10^6 g (PE)·mol^{-1}(Ni)·h^{-1}] and retained superior thermal stability at elevated temperatures. At 80 °C, **Ni1**/EASC maintained 75% higher activity [4.82 × 10^6 vs. 2.76 × 10^6 g (PE)·mol^{-1}(Ni)·h^{-1}], underscoring the beneficial influence of EASC as co-catalyst on the thermal stability of the catalytic system. Moreover, due to enhanced chain transfer rate at higher temperatures, the molecular weight of PEs falls as temperature increases: At 80 °C, M_w drops by 54% for **Ni1**/EASC and by 63% for **Ni1**/$EtAlCl_2$ compared with their values at 30 °C (Figure 2b).

Table 4. Ethylene polymerization with **Ni1**–**Ni5**/EASC [a].

Run	Precat.	Al/Ni	T (°C)	T (min)	PE (g)	Activity [b]	M_w [c]	M_w/M_n [c]	T_m [d] (°C)
1	**Ni1**	300	30	30	4.39	8.78	7.54	2.48	99.6
2	**Ni1**	300	40	30	10.7	21.4	6.41	3.59	58.7
3	**Ni1**	300	50	30	8.41	16.8	5.92	4.62	51.9
4	**Ni1**	300	60	30	6.18	12.4	4.71	2.64	51.6
5	**Ni1**	300	70	30	3.04	6.08	3.61	3.97	39.8
6	**Ni1**	300	80	30	2.41	4.82	3.44	3.08	32.9
7	**Ni1**	250	40	30	9.74	19.5	5.90	3.69	65.2
8	**Ni1**	350	40	30	11.0	22.0	6.15	3.50	59.2
9	**Ni1**	400	40	30	9.85	19.7	7.12	3.40	65.2
10	**Ni1**	450	40	30	8.83	17.7	7.16	3.80	56.7
11	**Ni1**	350	40	5	2.77	33.2	3.59	3.12	79.9
12	**Ni1**	350	40	15	6.47	25.9	5.10	3.04	83.9
13	**Ni1**	350	40	45	12.8	17.1	6.55	5.08	94.4
14	**Ni1**	350	40	60	13.4	13.4	7.78	3.09	72.7
15 [e]	**Ni1**	350	40	30	5.18	10.4	4.29	2.62	72.5
16 [f]	**Ni1**	350	40	30	0.86	1.72	3.70	2.17	- [g]
17	**Ni2**	350	40	30	7.41	14.8	5.10	3.32	81.2
18	**Ni3**	350	40	30	6.28	12.6	5.06	3.32	59.8
19	**Ni4**	350	40	30	7.11	14.2	3.84	2.87	78.2
20	**Ni5**	350	40	30	8.61	17.2	3.47	3.74	68.3

[a] Conditions: 1.0 µmol pre-catalyst, 100 mL of toluene, 10 atm C_2H_4; [b] 10^6 g (PE) mol^{-1} (Ni) h^{-1}; [c] M_w: $\times 10^5$ g mol^{-1}, M_w and M_w/M_n determined by GPC; [d] Determined by DSC; [e] 5 atm C_2H_4; [f] 1 atm C_2H_4; [g] Broad and weak endotherms, amorphous polymers.



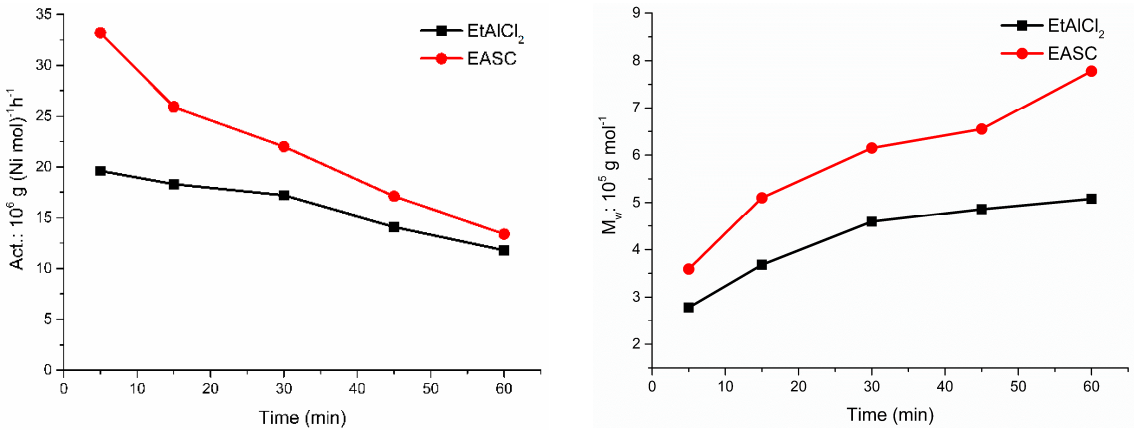
(**a**) (**b**)

Figure 2. Temperature-dependent (**a**) activity and (**b**) molecular weight trends using **Ni1**/EASC vs. **Ni1**/$EtAlCl_2$.

Next, we set the reaction temperature to 40 °C and varied the Al:Ni molar ratio from 250:1 to 450:1 to examine the impact of co-catalyst concentration on polymerization performance (runs 2, 7–10, Table 4). The activity peaked at 350:1 [22.0 × 10^6 g PE mol^{-1} (Ni) h^{-1}], higher than the optical ratio for $EtAlCl_2$ (200:1), attributed to the distinct properties of the two alkylaluminum reagents in EASC. Notably, this activity value surpasses most reported for *N*,*N*′-nickel catalysts under similar reaction conditions [24,35−45], except for one cycloalkyl substituted analog [22]. At an Al/Ni ratio of 450:1, the PE's relative molecular weight reached its maximum value of 7.16 × 10^5 g mol^{-1}.

Under optimal conditions, **Ni1**/EASC exhibits significantly faster initial activation (33.2 × 10^6 vs. 19.6 × 10^6 g PE mol^{-1}(Ni) h^{-1} 5 min) but accelerated deactivation (60% activity loss at 60 min) compared to **Ni1**/$EtAlCl_2$ (40% loss) (Figure 3a). Despite this,

Ni1/EASC consistently yielded PE with higher molecular weight (runs 8, 11–14, Table 4) than **Ni1**/$EtAlCl_2$ (e.g., 7.78×10^5 vs. 5.08×10^5 g mol^{-1} at 60 min; Figure 3b), underscoring its superior propagation efficiency under similar conditions. Likewise, reducing ethylene pressure diminishes both activity and polymer molecular weight in the **Ni1**/EASC system (runs 8, 15–16, Table 4), mirroring trends observed for **Ni1**/$EtAlCl_2$.



(**a**) (**b**)

Figure 3. Time-dependent (**a**) activity decay and (**b**) molecular weight evolution using **Ni1**/EASC vs. **Ni1**/$EtAlCl_2$.

Having identified the optimal reaction conditions for **Ni1**/EASC (Al:Ni = 350:1, 30 °C, 30 min, 10 atm ethylene), we further investigated the influence of ligand structural variations on polymerization performance (runs 2, 17–20, Table 4). The activity of the nickel complexes decreased in the following order: **Ni1** > **Ni5** > **Ni2** ≈ **Ni4** > **Ni3**. While the reasons behind these activity variations remain unclear, it is possible that different counteranions generated during catalyst activation affect the solubility of the complexes. Additionally, the electron-donating methyl group at the para-position of the *N*-aryl substituent appears to negatively affect polymer molecular weight, a phenomenon previously reported [45].

Building on prior findings that solvents critically influence polymerization reactions [39], we explored the impact of *n*-hexane versus toluene on **Ni1**/EASC (Table 5).

Table 5. Solvent effect on **Ni1**/EASC performance [a].

Run	Al/Ni	T (°C)	T (min)	PE (g)	Activity [b]	M_w [c]	M_w/M_n [c]	T_m [d] (°C)
1	350	40	30	1.23	2.46	8.24	3.65	116.8
2	450	40	30	5.22	10.4	7.36	3.60	114.7
3	500	40	30	6.16	12.3	6.63	3.52	104.9
4	550	40	30	6.87	13.7	6.09	3.60	110.3
5	600	40	30	3.79	7.58	7.63	3.80	119.7
6	550	30	30	4.00	8.00	11.1	2.33	118.4
7	550	50	30	6.01	12.0	3.05	3.31	107.4

[a] Conditions: 1.0 µmol **Ni1**, 100 mL of hexane, 10 atm C_2H_4; [b] 10^6 g (PE) mol^{-1} (Ni) h^{-1}; [c] M_w: $\times 10^5$ g mol^{-1}, M_w and M_w/M_n determined by GPC; [d] Determined by DSC.

Using identical optimal reaction conditions (Al:Ni = 350:1, 40 °C, 30 min, 10 atm ethylene), replacing toluene with n-hexane noticeably reduced catalytic activity [hexane: 2.46×10^6 vs. toluene: 22.0×10^6 g PE mol^{-1} (Ni) h^{-1}] but increased polymer molecular weight [hexane: 8.24×10^5 vs. toluene: 6.15×10^5 g mol^{-1}]. Further optimization the polymerization using hexane as the solvent showed catalytic activity peaked at 13.7×10^6 g PE mol^{-1} (Ni) h^{-1} when Al:Ni = 550:1 at 40 °C, though still lower than the

maximum activity observed in toluene. The cause of this behavior remains uncertain, it may be due to solvent-induced changes in catalyst solubility, solvent polarity, ligand electronic effects, and the ethylene coordination environment. Additionally, polymers synthesized in n-hexane exhibited higher melting points (e.g., 116.8 °C in n-hexane vs. 59.5 °C in toluene, Al/Ni = 350, T = 40 °C), suggesting reduced branching (*vide infra*).

2.3. Systematic Investigation of Substituent Effects on Catalytic Performance

2.3.1. Role of the *para*-Trifluoromethoxy (-OCF_3) Group

To clarify the impact of the *para*-trifluoromethoxy (-OCF_3) group on catalytic activity and molecular weight of the polymer, we compared **Ni1** with two reported asymmetric bis(arylimino)acenaphthene-nickel(II) bromide complexes (**D**, Chart 1) bearing *para*-OMe [42] and *para*-NO_2 [45] substituents (Figure 4). All polymerization reactions shown in the figure were carried out under identical conditions (EASC co-catalyst, toluene, 30 °C, and 10 atm ethylene).

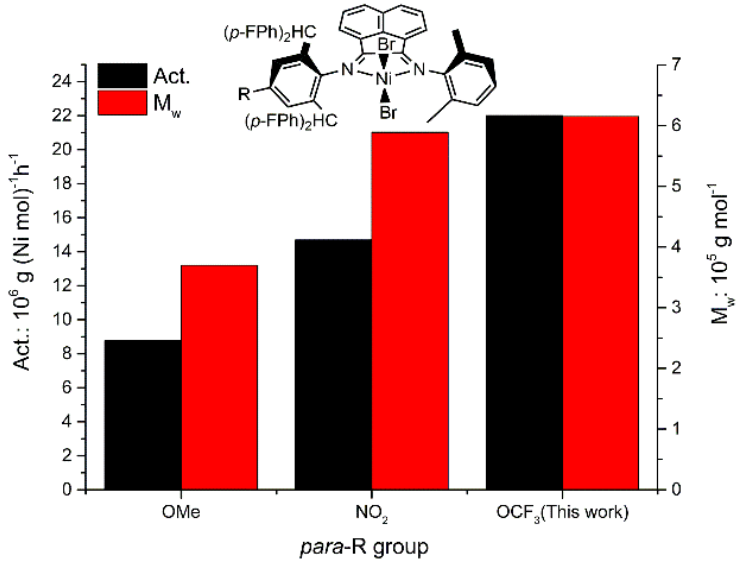


Figure 4. Comparison of activity and M_w of the PE generated by **Ni1** (R = OCF_3) with precatalyst **D** (Chart 1, R = OMe [35], NO_2 [36]) under identical conditions (EASC, 40 °C, P_{C2H4} = 10 atm, toluene).

From Figure 4, it is clear that introducing an -OCF_3 group at the para-position significantly enhances catalytic activity: **Ni1** achieved 22.0 × 10^6 g PE mol^{-1} (Ni) h^{-1} at 40 °C, nearly three times that of its para-methoxy (-OMe) analog. This improvement is due to the strong electron-withdrawing nature of the *para*-OCF_3, which likely polarizes the nickel center, facilitating ethylene coordination and insertion. In contrast, the *para*-nitro (-NO_2) analog exhibited reduced activity attributed to stronger electron-withdrawing of -NO_2, which impedes ethylene insertion [45]. Regarding PE molecular weight, all three nickel complexes in Figure 4 produced high molecular weight PEs (10^5 g mol^{-1}), suggesting that the *ortho*-bulky substituents help promote chain growth while effectively suppressing chain-transfer reaction [37]. Among them, the complex with the -OCF_3 group generated the highest molecular weight PE at 6.15 × 10^5 g mol^{-1}, emphasizing the promoting effect of this strongly electron-withdrawing group on ethylene insertion [45].

2.3.2. Effects of the Distal Fluorine Atom

To isolate the influence of the distal fluorine substituent, we compared **Ni1** with its non-fluorinated analog **C** [39] (Chart 1) under identical conditions (Figure 5). We found that **Ni1** bearing the distal fluorine exhibits markedly enhanced catalytic activity and remains highly efficient for ethylene polymerization at the industrially relevant temperature (70 °C),

presumably due to the enhanced Lewis acidity of the active metal species, leading to more efficient ethylene coordination and insertion. This demonstrates the positive role of the fluorine atom in boosting the catalyst's thermal stability and suggests excellent prospects for industrial application. In terms of polymer molecular weight, introduction of the distal F atom causes a slight decrease in the resulting PE's molecular weight, which may attribute to participant of the distal F atoms in chain-terminating interactions via weak C–H···F interactions with the growing polymer chain or solvent. This observation is consistent with previous study [56]. However, due to the bulky ortho substituent and the strongly electron-withdrawing *para*-trifluoromethoxy group, the obtained PE still maintains M_w on the order of 10^5 g mol^{-1}.

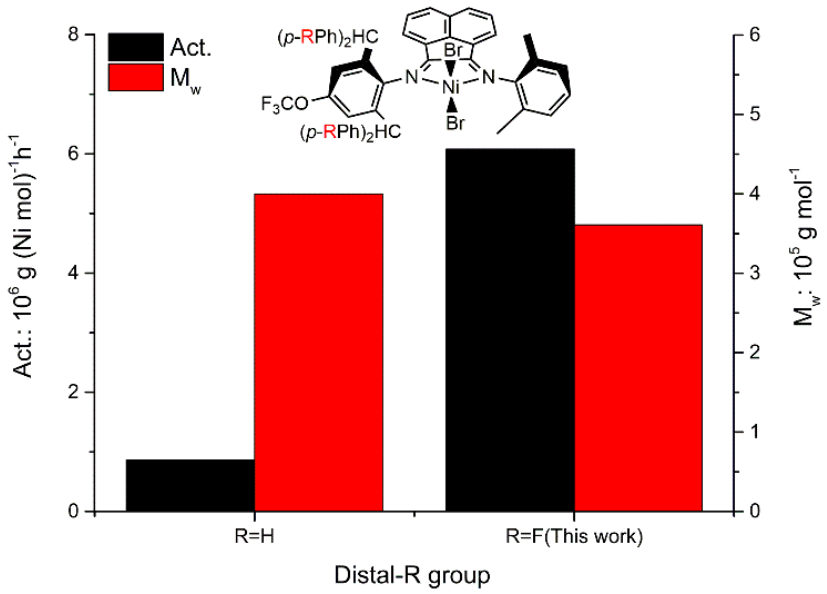


Figure 5. Comparison of activity and M_w of the PE generated by **Ni1** (R = F) with precatalyst **C** (Chart 1, R = H [43]) under identical conditions (EASC, 70 °C, Al/Ni = 300, P_{C2H4} = 10 atm, toluene).

In summary, by employing a dual-modification strategy with introducing trifluoromethoxy group and distal fluorine substituents, we have dramatically enhanced the activity and thermal stability of the pre-catalyst, enabling efficient ethylene polymerization at industrially relevant temperatures to yield high-molecular-weight PEs.

2.4. Branching Properties of the PEs

All PEs synthesized in this study have melting temperatures (T_m) below 120 °C, characteristic of branched PE (Tables 2–5). To quantify the effects of temperature, solvent, co-catalyst type and concentration on branching density and topology, ^{13}C NMR spectroscopy (measured at 100 °C, using $C_6D_4Cl_2$ as solvent) was used to analyze selected PE samples (Figure 6 and Figures S27–S31). From these spectra, characteristic signals corresponding to distinct carbon environments in the polymer chain and branches were identified, with results shown in Table 6.

A comparative analysis of PE samples synthesized with $EtAlCl_2$ (PE-40$_{EADC/300/T}$, PE-60$_{EADC/300/T}$) and EASC PE-40$_{EASC/300/T}$, and PE-60$_{EASC/300/T}$ revealed that increasing polymerization temperature elevated the degree of branching, while reducing the methyl branch content and promoting other types of branches. This indicates that higher temperatures favor chain walking, which leads to the formation of longer and more complex branched structures [57].

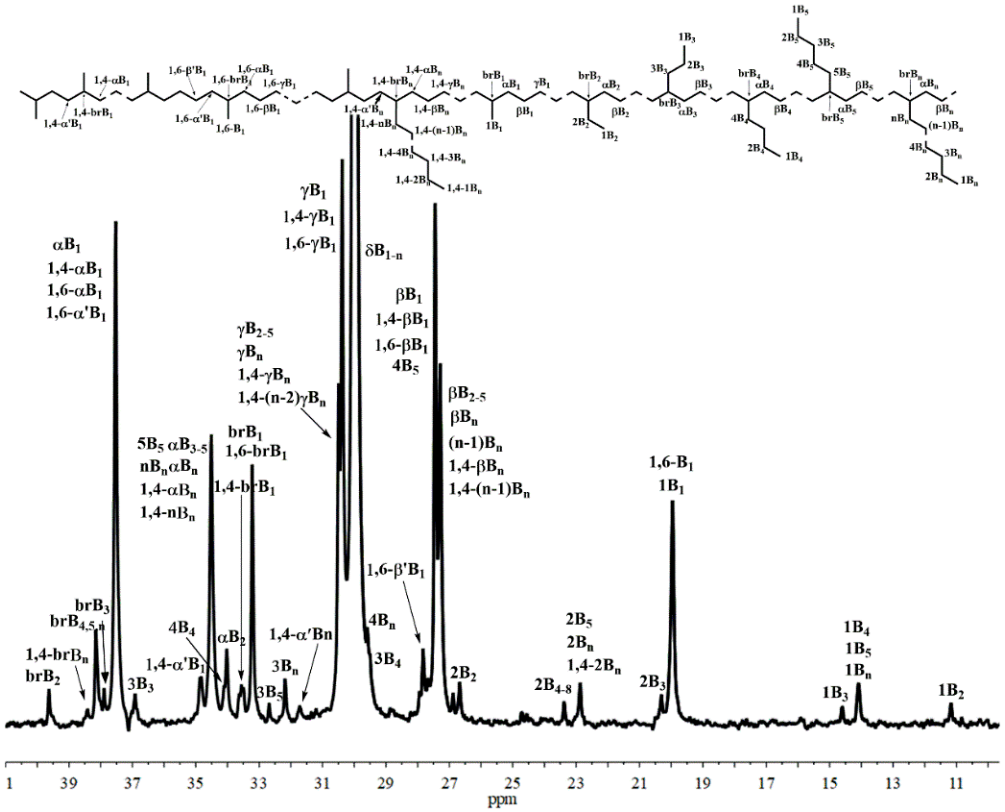


Figure 6. ^{13}C NMR spectrum of PE-40$_{EADC/300/T}$ along with a segment of the assigned polymer backbone; recorded in $C_6D_4Cl_2$ at 100 °C.

Table 6. Branching analysis of selected PE samples [a].

PE Sample [b]	Branches/ 1000 C's	Methyl Branches/%	Ethyl Branches/%	Propyl Branches/%	Butyl Branches/%	Amyl Branches/%	Longer Branches/%
PE-40$_{EADC/300/T}$	96.5	77.0	5.21	5.50	3.52	2.59	6.17
PE-60$_{EADC/300/T}$	128	70.2	7.29	6.92	5.23	3.04	7.31
PE-40$_{EASC/300/T}$	90.5	80.8	5.63	5.18	3.71	1.07	3.56
PE-60$_{EASC/300/T}$	107	79.4	5.46	5.26	3.26	1.62	5.03
PE-40$_{EASC/450/T}$	102	77.3	5.60	5.75	3.10	3.03	5.21
PE-40$_{EASC/450/H}$	52.6	83.0	4.83	3.70	1.81	1.55	5.10

[a] Data determined from the ^{13}C NMR spectrum using approaches described by G. B. Galland [58]; [b] Naming example: PE-40$_{EADC/300/T}$: 40 °C, $EtAlCl_2$, Al:Ni = 300, toluene.

Compared to $EtAlCl_2$, PE produced with EASC as a co-catalyst exhibited a lower degree of branching and lower long-chain content. In terms of the co-catalyst concentration, as Al:Ni increased from 300 to 450, the degree of branching in the resulting polymer increased (90.5 to 102 branches/1000 C), which explains why PE-40$_{EASC/450/T}$ has a lower melting point (56.7 vs. 58.7 °C) despite a higher molecular weight (7.16 vs. 6.41 × 10^5 g mol^{-1}; Table 4 run 10 vs. Run 2). Clearly, the choice of solvent affects the degree of branching: under the same conditions, samples obtained in toluene exhibited higher branching (102 branches/1000 C) than those obtained in hexane (52.6 branches/1000 C). This is contrasts to previously reported findings [39], and it seems that the introduction of distal fluorine substituent may perturb solvent-polymer interactions or chain-transfer pathways, though the underlying cause of this phenomenon requires further investigation.

2.5. Mechanical Properties of the PE

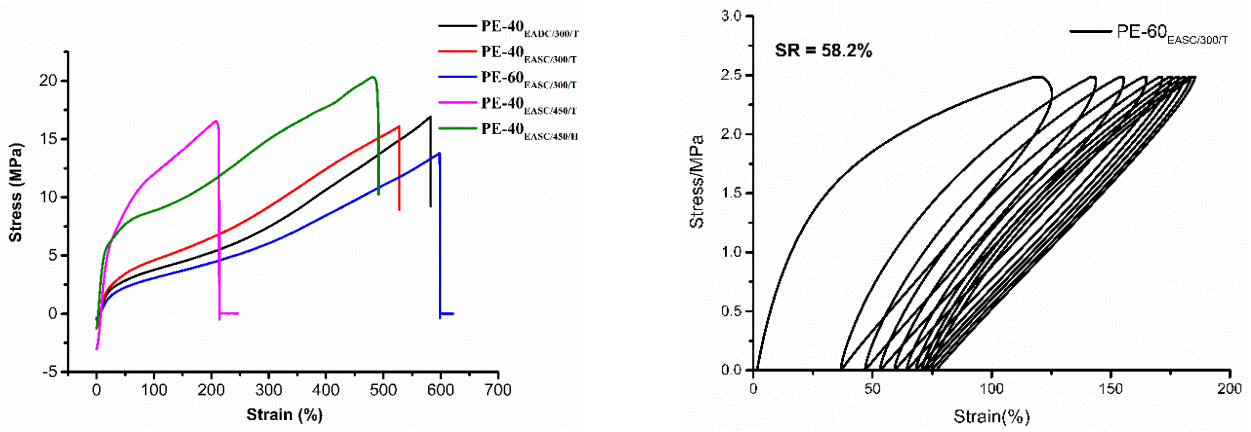
To explore the mechanical properties of these branched polymers, five samples—PE-$_{40EADC/300/T}$ (run 2, Table 3), PE-40$_{EASC/300/T}$ (run 2, Table 4), PE-60$_{EASC/300/T}$ (run

4, Table 4), PE-40$_{EASC/450/T}$ (run 10, Table 4), and PE-40$_{EASC/450/H}$ (run 2, Table 5) were subjected to monotonic tensile stress–strain testing. Five specimens of each sample were tested, and the average results were calculated to ensure statistical reliability. The tensile test data are shown in Table 7, and the stress–strain curves and hysteresis loops are provided in Figure 7.

Table 7. Stress strain properties of the selected PE samples.

PE Sample	T_m (°C) [a]	M_w [b]	Branches/1000 C's	X_c [a] (%)	Stress (MPa) [c]	Strain (%) [c]
PE-40$_{EADC/300/T}$	61.6	4.78	96.5	23.2	16.4	585
PE-40$_{EASC/300/T}$	58.7	6.41	90.5	22.3	15.3	482
PE-60$_{EASC/300/T}$	51.6	4.71	107	17.0	13.7	572
PE-40$_{EASC/450/T}$	56.7	7.16	102	19.5	16.8	237
PE-40$_{EASC/450/H}$	114.7	7.36	52.6	43.4	20.7	439

[a] Determined by DSC, $X_c = 100 \times \Delta H_f (T_m)/[\Delta H^\circ_f (T^\circ_m)]$, where $\Delta H^\circ_f (T^\circ_m) = 248.3$ J g^{-1}; [b] M_w ($\times 10^5$ g mol^{-1}), determined by GPC; [c] Determined using a universal testing instrument.



(**a**) (**b**)

Figure 7. (**a**) Stress–strain curves for PE-40$_{EADC/300/T}$, PE-40$_{EASC/300/T}$, PE-60$_{EASC/300/T}$, PE-40$_{EASC/450/T}$, and PE-40$_{EASC/450/H}$ obtained during monotonic tensile deformation; (**b**) Hysteresis loops for PE-60$_{EASC/300/T}$ obtained using ten cycles at 30 °C.

We found that these polymers exhibited superior tensile strength compared to those previously reported using nickel-catalysted systems [19,20,35,39,41,50]. In terms of the effects of polymerization conditions, PE-40$_{EADC/300/T}$ (activated with $EtAlCl_2$) and PE-40$_{EASC/300/T}$ (activated with EASC) showed comparable tensile strengths, but PE-40$_{EADC/300/T}$, which had a higher degree of branching (96.5 vs. 90.5 branches/1000 C), demonstrated a higher elongation at break (585% vs. 482%). For samples obtained at higher temperatures, crystallinity decreased to 17.0%, resulting in a reduction in tensile strength to 13.7 MPa, while elongation at break increased to 572%. On the other hand, when n-hexane was used as the solvent instead of toluene, PE-40$_{EASC/450/H}$ exhibited improvements in both tensile strength (20.7 MPa) and elongation at break (439%) compared to PE-40$_{EASC/450/T}$. These results indicate that polymer molecular weight, crystallinity, and branching structure significantly influence the tensile properties of PE.

Finally, to assess the elastic recovery performance of the polymers, dynamic mechanical analysis (DMA) was used to perform hysteresis tests on PE-60$_{EASC/300/T}$. The tests were conducted at 30 °C, with each cycle repeated 10 times, as shown in Figure 7b. The elastic recovery rate (SR) was calculated using the standard formula $SR = 100(\varepsilon_a - \varepsilon_r)/\varepsilon_a$, where ε_a is the applied strain, and ε_r is the strain after 10 cycles at zero load. Notably, after 10 cycles, the sample retained good elastic recovery performance with an SR of 58.2%,

which can be attributed to the high degree of branching and the relatively high content of long branches in the PE [35]. In summary, these PE samples demonstrated excellent tensile strength, elongation at break, and elastic recovery, making them potential substitutes for commercial thermoplastic elastomers.

3. Materials and Methods

3.1. Synthesis of 2-(2,6-Bis(bis(4-fluorophenyl)methyl)-4-trifluoromethoxy)acenaphthylen-1-one

To a mixture of 2,6-bis(4,4′-difluorobenzhydryl)-4-(trifluoromethoxy)aniline (4.65 g, 8 mmol), acenaphthylene-1,2-dione (1.60 g, 8.8 mmol), and a catalytic amount of *p*-toluenesulfonic acid (1.25 g), toluene (30 mL) was added. The resulting solution was refluxed for 5.5 h. After the reaction, all volatiles were removed under reduced pressure, and the residue was purified by alumina column chromatography (500/8 petroleum ether/ethyl acetate). The product was obtained as a yellow powder (3.76 g, 63.0%). ^{1}H NMR (400 MHz, $CDCl_3$, TMS): δ 8.13–8.08 (m, 2H), 7.86 (d, *J* = 8.4 Hz, 1H), 7.78 (t, *J* = 7.8 Hz, 1H), 7.10 (t, *J* = 7.8 Hz, 1H), 6.95 (d, *J* = 6.8 Hz, 9H), 6.81 (s, 2H), 6.79–6.75 (m, 4H), 6.31 (t, *J* = 8.4 Hz, 3H), 5.99 (d, *J* = 6.8 Hz, 1H), 5.40 (s, 2H). ^{13}C NMR (100MHz, $CDCl_3$, TMS): δ 188.98, 162.98, 162.88, 162.07, 160.44, 159.62, 146.49, 145.81, 142.54, 137.24, 137.12, 136.38, 136.35, 133.82, 132.66, 132.52, 131.27, 131.20, 130.93, 130.86, 130.72, 130.64, 130.56, 130.07, 129.99, 129.53, 129.47, 128.48, 128.14, 127.04, 126.19, 123.34, 122.27, 122.12, 121.53, 120.85, 119.17, 115.88, 115.67, 115.49, 115.28, 115.20, 114.99, 50.51.

*3.2. Synthesis of Ligands (***L1**–**L5***)*

L1. To a mixture of 2-(2,6-bis(4,4′-difluorobenzhydryl)-4-trifluoromethoxy) acenaphthylen-1-one (1.49 g, 2.0 mmol), 2,6-dimethylaniline (0.36 g, 3.0 mmol), and a catalytic amount of p-toluenesulfonic acid (0.37 g), toluene (30 mL) was added. The resulting solution was refluxed for 6 h. After the reaction, all volatiles were removed under reduced pressure, and the residue was purified by alumina column chromatography (500/8 petroleum ether/ethyl acetate). The product was obtained as a yellow powder (0.49 g, 27.6%). ^{1}H NMR (400 MHz, $CDCl_3$, TMS): δ 7.82 (d, *J* = 8.4 Hz, 1H, An-H), 7.75 (d, *J* = 8.0 Hz, 1H, An-H), 7.33 (t, *J* = 7.6 Hz, 1H, An-H), 7.19 (d, *J* = 7.6 Hz, 2H, Ar-H), 7.13–7.09 (m, 1H, Ar-H), 7.06 (t, *J* = 7.6 Hz, 1H, An-H), 7.02–6.94 (m, 8H, Ar-H), 6.87–6.82 (m, 6H, Ar-H), 6.59 (d, *J* = 7.2 Hz, 1H, An-H), 6.32 (t, *J* = 8.4 Hz, 1H, Ar-H), 5.98 (d, *J* = 7.2 Hz, 1H, An-H), 5.59 (s, 2H, -C*H*Ph_2), 2.19 (s, 6H, -CH_3). ^{13}C NMR (100MHz, $CDCl_3$, TMS): δ 164.2, 162.9, 162.0, 161.1, 160.4, 159.6, 148.8, 147.4, 145.4, 139.9, 137.5, 137.5, 136.5, 136.5, 134.2, 131.1, 131.0, 130.7, 130.6, 130.1, 129.3, 129.2, 128.5, 128.3, 128.1, 127.9, 126.7, 124.5, 124.1, 123.6, 122.4, 121.8, 120.9, 119.2, 115.4, 115.2, 115.1, 114.9, 50.9, 50.6, 18.1. ^{19}F NMR (470 MHz, $CDCl_3$, TMS): δ −58.17, −116.12, −116.35. FT-IR (cm^{-1}): 3074 (w), 3043 (w), 2977 (w), 2941 (w), 1662 (m, $\upsilon_{C=N}$), 1635 (w, $\upsilon_{C=N}$), 1697 (m), 1506 (s), 1465 (w), 1440 (m), 1257 (w), 1217 (w), 1159 (w), 1095 (w), 1040 (w), 1012 (w), 928 (w), 875 (w), 828 (m), 802 (w), 769 (m). Anal. calcd for $C_{53}H_{35}F_7N_2O{\cdot}H_2O$ (848.86): C, 74.99; H, 4.16; N, 3.30. Found: C, 75.24; H, 4.10; N, 3.11%.

L2. Using a typical procedure as described for the synthesis of **L1**, **L2** was prepared as a yellow powder (0.51 g, 29.1%). ^{1}H NMR (400 MHz, $CDCl_3$, TMS): δ 7.80 (d, *J* = 8.0 Hz, 1H), 7.71 (d, *J* = 8.4 Hz, 1H), 7.31 (t, *J* = 7.8 Hz, 1H), 7.25–7.20 (m, 3H), 7.02–6.94 (m, 9H), 6.86–6.83 (m, 6H), 6.58 (d, *J* = 7.2 Hz, 1H), 6.30 (t, *J* = 8.6 Hz, 4H), 5.88 (d, *J* = 7.2 Hz, 1H), 5.60 (s, 2H), 2.70–2.61 (m, 2H), 2.54–2.45 (m, 2H), 1.17 (t, *J* = 7.4 Hz, 6H). ^{13}C NMR (100MHz, $CDCl_3$, TMS): δ 162.9, 162.0, 161.2, 160.4, 159.6, 147.9, 147.5, 139.9, 137.8, 136.5, 136.4, 134.2, 131.0, 130.7, 130.6, 130.4, 130.00, 129.2, 129.0, 128.3, 127.8, 126.6, 126.4, 124.5, 123.7, 122.9, 121.0, 115.4, 115.2, 115.1, 114, 9, 50.6, 24.5, 14.4. ^{19}F NMR (470 MHz, $CDCl_3$, TMS): δ −58.18, −116.13, −116.33. FT-IR (cm^{-1}): 3053 (w), 2966 (w), 2937 (w), 2878 (w), 1672 (w, $\upsilon_{C=N}$), 1654 (w, $\upsilon_{C=N}$), 1598 (w), 1506 (s), 1437 (m), 1253 (w), 1224 (w), 1159 (w), 1095 (w), 1042

(w), 1014 (w), 923 (w), 875 (w), 828 (w), 802(w), 782 (w). Anal. calcd for $C_{55}H_{39}F_7N_2O{\cdot}H_2O$ (876.92): C, 75.33; H, 4.48; N, 3.19. Found: C, 75.65; H, 4.32; N, 2.87%.

L3. Using a typical procedure as described for the synthesis of **L1**, **L3** was prepared as a yellow powder (0.44 g, 24.1%). ^{1}H NMR (400 MHz, $CDCl_3$, TMS): δ 7.78 (d, *J* = 8.4 Hz, 1H), 7.68 (d, *J* = 8.4 Hz, 1H), 7.33–7.29 (m, 4H, An-H), 7.02–6.93 (m, 9H), 6.85–6.82 (m, 6H), 6.48 (d, *J* = 7.2 Hz, 1H), 6.27 (t, *J* = 8.6 Hz, 4H), 5.79 (d, *J* = 7.2 Hz, 1H), 5.61 (s, 2H), 3.14–3.04 (m, 2H), 1.29 (d, *J* = 6.8 Hz, 6H), 1.01 (d, *J* = 6.8 Hz, 6H). ^{13}C NMR (100MHz, $CDCl_3$, TMS): δ 164.4, 162.9, 162.0, 161.8, 160.4, 159.6, 147.6, 146.7, 145.5, 139.9, 137.9, 136.4, 135.4, 134.3, 131.0, 130.8, 130.7, 130.0, 129.3, 128.9, 128.2, 127.7, 127.5, 126.6, 124.9, 123.8, 123.4, 121.1, 115.4, 115.2, 115.0, 50.6, 28.7, 24.2, 23.7. ^{19}F NMR (470 MHz, $CDCl_3$, TMS): δ −58.19, −116.12, −116.28. FT-IR (cm^{-1}): 3053 (w), 2965 (w), 2932 (w), 2876 (w), 1671 (w, $\upsilon_{C=N}$), 1649 (w, $\upsilon_{C=N}$), 1598 (w), 1506 (s), 1436 (w), 1392 (w), 1361 (w), 1333 (w), 1300 (w), 1228 (w), 1165 (w), 1095 (w), 1041 (w), 1014 (w), 923 (w), 876 (w), 830 (m), 785 (w), 761 (w). Anal. calcd for $C_{57}H_{43}F_7N_2O{\cdot}H_2O$ (904.97): C, 75.65; H, 4.79; N, 3.10. Found: C, 75.37; H, 5.06; N, 3.44%.

L4. Using a typical procedure as described for the synthesis of **L1**, **L4** was prepared as a yellow powder (0.66 g, 38.0%). ^{1}H NMR (400 MHz, $CDCl_3$, TMS): δ 7.81 (d, *J* = 8.0 Hz, 1H), 7.74 (d, *J* = 8.4 Hz, 1H), 7.34 (t, *J* = 7.8 Hz, 1H), 7.07–6.93 (m, 11H), 6.86–6.82 (m, 6H), 6.66 (d, *J* = 7.2 Hz, 1H), 6.32 (t, *J* = 8.6 Hz, 4H), 5.98 (d, *J* = 6.8 Hz, 1H), 5.58 (s, 2H), 2.39 (s, 3H), 2.15 (s, 6H). ^{13}C NMR (100MHz, $CDCl_3$, TMS): δ 164.2, 162.9, 162.1, 161.2, 160.5, 159.6, 147.5, 146.4, 145.4, 139.9, 137.6, 136.6, 134.2, 133.4, 131.1, 131.0, 130.8, 130.7, 130.1, 129.2, 128.5, 128.1, 126.6, 124.3, 123.5, 122.4, 121.8, 120.9, 119.3, 115.4, 115.2, 115.1, 114.9, 50.9, 50.7, 20.9, 18.0. ^{19}F NMR (470 MHz, $CDCl_3$, TMS): δ −58.17, −116.16, −116.39. FT-IR (cm^{-1}): 3043 (w), 2975 (w), 2912 (w), 1668 (w, $\upsilon_{C=N}$), 1642 (w, $\upsilon_{C=N}$), 1599 (w), 1506 (m), 1482 (w), 1440 (w), 1256 (w), 1224 (w), 1155 (w), 1096 (w), 1035 (w), 1013 (w), 925 (w), 831 (m), 778 (m), 732 (w). Anal. calcd for $C_{54}H_{37}F_7N_2O{\cdot}H_2O$ (862.89): C, 75.17; H, 4.32; N, 3.25. Found: C, 75.56; H, 4.73; N, 3.09%.

L5. Using a typical procedure as described for the synthesis of **L1**, **L5** was prepared as a yellow powder (0.40 g, 22.5%). ^{1}H NMR (400 MHz, $CDCl_3$, TMS): δ 7.79 (d, *J* = 8.4 Hz, 1H), 7.70 (d, *J* = 8.4 Hz, 1H), 7.32 (t, *J* = 7.6 Hz, 1H), 7.04 (s, 2H), 7.02–6.94 (m, 9H), 6.86–6.82 (m, 6H), 6.64 (d, *J* = 7.2 Hz, 1H), 6.30 (t, *J* = 8.4 Hz, 4H), 5.87 (d, *J* = 7.2 Hz, 1H), 5.60 (s, 2H), 2.65–2.56 (m, 2H), 2.51–2.42 (m, 5H), 1.14 (t, *J* = 7.4 Hz, 6H). ^{13}C NMR (100MHz, $CDCl_3$, TMS): δ 164.2, 162.9, 162.1, 161.2, 160.4, 159.6, 147.5, 146.3, 145.4, 139.9, 137.6, 136.6, 134.2, 133.4, 131.1, 131.0, 130.7, 130.6, 130.1, 129.2, 129.1, 128.4, 128.0, 126.6, 124.3, 123.5, 122.4, 121.0, 115.4, 115.2, 115.0, 114.8, 50.8, 50.6, 20.9,18.0. ^{19}F NMR (470 MHz, $CDCl_3$, TMS): δ −58.18, −116.17, −116.38. FT-IR (cm^{-1}): 3048 (w), 2965 (w), 2918 (w), 2854 (w), 1661 (w, $\upsilon_{C=N}$), 1640 (w, $\upsilon_{C=N}$), 1598 (w), 1505 (m), 1463 (w), 1438 (w), 1256 (w), 1217 (w), 1152 (w), 1093 (w), 1042 (w), 1013 (w), 927 (w), 864 (w), 829 (w), 786 (w). Anal. calcd for $C_{56}H_{41}F_7N_2O{\cdot}H_2O$ (890.95): C, 75.49; H, 4.64; N, 3.14. Found: C, 75.12; H, 4.26; N, 3.54%.

*3.3. Synthesis of Nickel Complexes (***Ni1**–**Ni5***)*

Ni1. Under a nitrogen atmosphere, **L1** (0.10 g, 0.12 mmol), $NiBr_2$(DME) (0.04 g, 0.12 mmol), dichloromethane (6 mL), and ethanol (4 mL) were stirred at ambient temperature for 12 h. The solution was concentrated, and diethyl ether (25 mL) was added to precipitate the product. It was collected by filtration and washed with excess diethyl ether (3 × 15 mL) affording **Ni1** as a red powder (0.12 g, 92.1% yield). ^{1}H NMR (400 MHz, CD_2Cl_2, TMS): δ 28.48 (s, 6H, $-CH_3$), 25.39 (s, 2H, Ar-Hm), 25.06 (s, 1H, An-H), 21.81 (s, 2H, Ar-Hm), 18.74 (s, 1H, An-H), 16.90 (s, 1H, An-H), 16.06 (s, 1H, An-H), 11.91 (broad, 0.81H, $-CHPh_2F_2$), 8.16 (s, 4H, Ar-H), 7.07 (s, 4H, Ar-H), 6.31 (s, 1H, An-H), 5.46 (s, 4H, Ar-H), 5.05 (s, 1H, An-H), 1.25 (s, 4H, Ar-H), -16.17 (s, 1H, Ar-Hp). ^{19}F NMR (470 MHz,

$CDCl_3$, TMS): δ −57.12, −115.73, −116.07. FT-IR (cm^{-1}): 3071 (w), 3036 (w), 2972 (w), 2906 (w), 1649 (w, $v_{C=N}$), 1623 (w, $v_{C=N}$), 1601 (w), 1585 (w), 1506 (s), 1444 (w), 1421 (w), 1262 (w), 1221 (w), 1158 (m), 1096 (w), 1051 (w), 1014 (w), 959 (w), 878 (w), 834 (m), 773 (m). Anal. calcd for $C_{53}H_{35}Br_2F_7N_2NiO$ (1067.37): C, 59.64; H, 3.31; N, 2.62. Found: C, 60.01; H, 3.17; N, 2.35%.

Ni2. Using a typical procedure as described for the synthesis of **Ni1**, **Ni2** was also afforded as a red powder (0.11 g, 86.2% yield). ^{1}H NMR (400 MHz, $CDCl_3$, TMS): δ 28.89 (s, 2H, $-CH_2CH_3$), 27.44 (s, 2H, $-CH_2CH_3$), 25.69 (s, 1H, An-H), 25.51 (s, 2H, Ar-Hm), 22.31 (s, 2H, Ar-Hm), 19.48 (s, 1H, An-H), 17.36 (s, 1H, An-H), 16.52 (s, 1H, An-H), 13.21 (broad, 1.2H, $-CHPh_2F_2$), 8.20 (s, 4H, Ar-H), 7.07 (s, 4H, Ar-H), 6.09 (s, 1H, An-H), 5.54 (s, 4H, Ar-H), 4.97 (s, 1H, An-H), 1.79 (s, 2H, Ar-H), 1.22 (s, 1H, Ar-H), 0.81 (s, 7H, Ar-H, $-CH_2CH_3$), −16.87 (s, 1H, Ar-Hp). ^{19}F NMR (470 MHz, $CDCl_3$, TMS): δ −57.09, −115.67, −116.16. FT-IR (cm^{-1}): 3069 (w), 3046 (w), 2978 (w), 2942 (w), 1649 (w, $v_{C=N}$), 1621 (w, $v_{C=N}$), 1603 (w), 1583 (w), 1505 (s), 1440 (w), 1421 (w), 1293 (w), 1256 (w), 1217 (w), 1157 (w), 1104 (w), 1050 (w), 1014 (w), 958 (w), 877 (w), 831 (m), 771 (w), 729 (w). Anal. calcd for $C_{55}H_{39}Br_2F_7N_2NiO$ (1095.42): C, 60.31; H, 3.59; N, 2.56. Found: C, 60.11; H, 3.46; N, 2.78%.

Ni3. Using a typical procedure as described for the synthesis of **Ni1**, **Ni3** was also afforded as a red powder (0.11 g, 84.9% yield). ^{1}H NMR (400 MHz, $CDCl_3$, TMS): δ 26.25 (s, 1H, An-H), 25.16 (s, 2H, Ar-Hm), 22.75 (s, 2H, Ar-Hm), 2.10 (s, 1H, An-H), 17.89 (s, 1H, An-H), 16.72 (s, 1H, An-H), 13.80 (broad, 2H, $-CHPh_2F_2$), 8.14 (s, 4H, Ar-H), 7.02 (s, 4H, Ar-H), 6.85 (s, 1H, An-H), 5.68 (s, 6H, Ar-H), 4.97 (s, 1H, An-H), 1.87 (s, 7H, Ar-H, $-CH(CH_3)_2$), 1.69 (s, 6H, $-CH(CH_3)_2$), 1.30 (s, 1H, Ar-H), 1.03 (s, 2H, $-CH(CH_3)_2$), −16.41 (s, 1H, Ar-Hp). ^{19}F NMR (470 MHz, $CDCl_3$, TMS): δ −57.19, −115.91, −116.09. FT-IR (cm^{-1}): 3072 (w), 3038 (w), 2969 (w), 2913 (w), 1645 (w, $v_{C=N}$), 1620 (w, $v_{C=N}$), 1601 (w), 1582 (w), 1506 (s), 1442 (w), 1421 (w), 1390 (w), 1364 (w), 1328 (w), 1298 (w), 1261 (w), 1220 (w), 1159 (w), 1097 (w), 1050 (w), 1014 (w), 958 (w), 876 (w), 832 (m), 772 (w), 734 (w). Anal. calcd for $C_{57}H_{43}Br_2F_7N_2NiO$ (1123.47): C, 60.94; H, 3.86; N, 2.49. Found: C, 60.73; H, 3.52; N, 2.57%.

Ni4. Using a typical procedure as described for the synthesis of **Ni1**, **Ni4** was also afforded as a red powder (0.11 g, 87.8% yield). ^{1}H NMR (400 MHz, $CDCl_3$, TMS): δ 34.47 (s, 3H, Ar–p–CH_3), 29.31 (s, 6H, -CH_3), 25.92 (s, 1H, An-H), 25.31 (s, 2H, Ar-Hm), 22.07 (s, 2H, Ar-Hm), 19.14 (s, 1H, An-H), 17.23 (s, 1H, An-H), 16.40 (s, 1H, An-H), 12.71 (broad, 0.99H, $-CHPh_2F_2$), 8.18 (s, 4H, Ar-H), 7.07 (s, 4H, Ar-H), 6.20 (s, 1H, An-H), 5.47 (s, 4H, Ar-H), 4.92 (s, 1H, An-H), 1.26 (s, 2H, Ar-H), 1.07 (s, 2H, Ar-H). ^{19}F NMR (470 MHz, $CDCl_3$, TMS): δ −57.15, −115.78, −116.10. FT-IR (cm^{-1}): 3069 (w), 2991 (w), 2911 (w), 1643 (w, $v_{C=N}$), 1624 (w, $v_{C=N}$), 1602 (w), 1583 (w), 1505 (s), 1443 (w), 1269 (m), 1217 (m), 1191 (w), 1155 (m), 1096 (w), 1048 (w), 1015 (w), 962 (w), 877 (w), 832 (m), 777 (w). Anal. calcd for $C_{54}H_{37}Br_2F_7N_2NiO$ (1081.39): C, 59.98; H, 3.45; N, 2.59. Found: C, 60.26; H, 3.58; N, 2.27%.

Ni5. Using a typical procedure as described for the synthesis of **Ni1**, **Ni5** was also afforded as a red powder (0.12 g, 90.5% yield). ^{1}H NMR (400 MHz, $CDCl_3$, TMS): δ 34.75 (s, 3H, Ar–p–CH_3), 28.61 (s, 2H, $-CH_2CH_3$), 27.53 (s, 2H, $-CH_2CH_3$), 26.25 (s, 1H, An-H), 25.19 (s, 2H, Ar-Hm), 22.29 (s, 2H, Ar-Hm), 19.29 (s, 1H, An-H), 17.30 (s, 1H, An-H), 16.54 (s, 1H, An-H), 13.02 (broad, 1.2H, $-CHPh_2F_2$), 8.24 (s, 4H, Ar-H), 7.08 (s, 4H, Ar-H), 6.16 (s, 1H, An-H), 5.53 (s, 4H, Ar-H), 4.90 (s, 1H, An-H), 1.22 (s, 3H, Ar-H), 0.87 (s, 7H, Ar-H, $-CH_2CH_3$). ^{19}F NMR (470 MHz, $CDCl_3$, TMS): δ −58.16, −115.86, −116.09. FT-IR (cm^{-1}): 3079 (w), 2975 (w), 2935 (w), 2873 (w), 1644 (w, $v_{C=N}$), 1618 (w, $v_{C=N}$), 1602 (w), 1583 (w), 1504 (s), 1444 (w), 1383 (w), 1296 (w), 1252 (w), 1220 (w), 1174 (w), 1157 (w), 1098 (w), 1054 (w), 1015 (w), 960 (w), 868 (w), 831 (m), 773 (m), 731 (w). Anal. calcd for $C_{56}H_{41}Br_2F_7N_2NiO$ (1109.45): C, 60.63; H, 3.73; N, 2.53. Found: C, 60.48; H, 3.61; N, 2.88%.

4. Conclusions

In this study, a novel series of asymmetric 1,2-bis(imine)acenaphthene nickel(II) complexes (**Ni1**–**Ni5**) featuring para-trifluoromethoxy and distal-fluoro-benzhydryl groups, was developed. These dual-functionalized catalysts achieved exceptional ethylene polymerization activity (up to 22.0 $\times$ 10^6 g PE mol^{-1}(Ni) h^{-1}) and outstanding thermal stability, maintaining 4.82 $\times$ 10^6 g PE mol^{-1}(Ni) h^{-1} at 80 °C. The synergistic combination of electron-withdrawing trifluoromethoxy and sterically shielding fluorobenzhydryl groups enhanced both the electrophilicity of the nickel center and resistance to thermal deactivaton, enabling efficient ethylene polymerization under industrially relevant conditions. By systematically modulating ligand architecture and co-catalyst, solvent (toluene vs. n-hexane), and polymerization parameters (temperature, time, and ethylene pressure), we achieved precise control over PE branching density and molecular weight. The strong electron-withdrawing *para*-trifluoromethoxy group facilitates ethylene insertion, thereby increasing the molecular weight of the resultant polymer. Furthermore, the bulky *ortho*-substituent promotes chain growth and chain walking while effectively suppressing chain transfer reactions, leading to the formation of polyethylenes with high molecular weight and high branching density. The resulting PEs displayed highly branching levels alongside robust mechanical properties, including tensile strengths up to 20.7 MPa and 58% elastic recovery. Comprehensive characterization of ligands, complexes, and polymers revealed structure–property relationships critical for advancing TPEs production technologies. This work underscores the potential of rationally designed nickel catalysts for high-temperature ethylene polymerization processes, offering a versatile platform to tailor polyolefin architectures for advanced elastomeric applications, where the integration of fluorine-based substituents elevates catalytic efficiency and enables scalable production of high-performance thermoplastic elastomers (TPEs) with tunable mechanical properties.

Supplementary Materials: The following supporting information can be downloaded at: https://www.mdpi.com/article/10.3390/molecules30132706/s1. General Considerations [48], Table S1: Crystal data and structure refinement for **Ni2** and **Ni4** [59–61]; Figure S1–S15: $^1H/^{13}C/^{19}F$ NMR spectra of **L1**–**L5**; Figure S16–S25: $^1H/^{19}F$ NMR spectra of **Ni1**–**Ni5**; Figure S26: GPC traces of the PE's obtained using **Ni1**/$EtAlCl_2$; Figure S27–S31: ^{13}C NMR spectra of the selected PEs. References [59–61] are cited in the Supplementary Materials.

Author Contributions: Methodology, investigation, writing—original draft preparation, M.L. (Ming Liu); data curation, M.L. (Ming Liu) and M.S.; GPC analysis, writing—review and editing Y.M.; funding acquisition, M.L. (Mingfeng Li); X-Ray analysis, Y.W.; supervision, M.L. (Mingfeng Li) and W.-H.S.; resources, project administration, W.-H.S. All authors have read and agreed to the published version of the manuscript.

Funding: This research was funded by SINOPEC Research Institute of Petroleum Processing Co., Ltd. No. 36800000-23-ZC0699-0122 and the Strategic Priority Research Program of the Chinese Academy of Sciences, No. XDC0270102.

Institutional Review Board Statement: Not applicable.

Informed Consent Statement: Not applicable.

Data Availability Statement: CCDC reference numbers 2451477 and 2451478 contain supplementary crystallographic information for **Ni2** and **Ni4** (see Supplementary Materials), and the data presented in this study are available in this article.

Conflicts of Interest: The authors declare that this study received funding from SINOPEC Research Institute of Petroleum Processing Co., Ltd. and the Strategic Priority Research Program of the Chinese Academy of Sciences. The funder was not involved in the study design, collection, analysis, interpretation of data, the writing of this article or the decision to submit it for publication.

References

1. Braunecker, W.A.; Matyjaszewski, K. Controlled/living radical polymerization: Features, developments, and perspectives. *Prog. Polym. Sci.* **2007**, *32*, 93–146. [CrossRef]
2. Zanchin, G.; Leone, G. Polyolefin Thermoplastic Elastomers from Polymerization Catalysis: Advantages, Pitfalls and Future Challenges. *Prog. Polym. Sci.* **2021**, *113*, 101342. [CrossRef]
3. Adhikari, B.; De, D.; Maiti, S. Reclamation and recycling of waste rubber. *Prog. Polym. Sci.* **2000**, *25*, 909. [CrossRef]
4. Dow Chemical Company. Olefin Solution Polymerization. WO1997036942A1, 9 October 1997.
5. Chatterjee, A.M. *Handbook of Industrial Polyethylene and Technology Definitive Guide to Manufacturing, Properties, Processing, Applications and Markets*; John Wiley & Sons Inc.: Hoboken, NJ, USA, 2017; pp. 124–125.
6. Exxon Chemical Patents Inc. Process and Catalyst for Polyolefin Density and Molecular Weight Control. US, 5324800A, 28 June 1994.
7. Johnson, L.K.; Killian, C.M.; Brookhart, M. New Pd(II)- and Ni(II)-Based Catalysts for Polymerization of Ethylene and α-Olefins. *J. Am. Chem. Soc.* **1995**, *117*, 6414–6415. [CrossRef]
8. Killian, C.M.; Tempel, D.J.; Johnson, L.K.; Brookhart, M. Living Polymerization of α-Olefins Using Ni^{II}-α-Diimine Catalysts. Synthesis of New Block Polymers Based on α-Olefins. *J. Am. Chem. Soc.* **1996**, *118*, 11664–11665. [CrossRef]
9. Leatherman, M.D.; Svejda, S.A.; Johnson, L.K.; Brookhart, M. Mechanistic Studies of Nickel(II) Alkyl Agostic Cations and Alkyl Ethylene Complexes: Investigations of Chain Propagation and Isomerization in (α-diimine)Ni(II)-Catalyzed Ethylene Polymerization. *J. Am. Chem. Soc.* **2003**, *125*, 3068–3290. [CrossRef]
10. Michalak, A.; Ziegler, T. Polymerization of Ethylene Catalyzed by a Nickel(+2) Anilinotropone-Based Catalyst: DFT and Stochastic Studies on the Elementary Reactions and the Mechanism of Polyethylene Branching. *Organometallics* **2003**, *22*, 2069–2079. [CrossRef]
11. Falivene, L.; Wiedemann, T.; Göttker-Schnetmann, I.; Caporaso, L.; Cavallo, L.; Mecking, S. Control of Chain Walking by Weak Neighboring Group Interactions in Unsymmetrical Catalysts. *J. Am. Chem. Soc.* **2018**, *140*, 1305–1312. [CrossRef]
12. O'Connor, K.S.; Lamb, J.R.; Vaidya, T.; Keresztes, I.; Klimovica, K.; LaPointe, A.M.; Daugulis, O.; Coates, G.W. Understanding the Insertion Pathways and Chain Walking Mechanisms of α-Diimine Nickel Catalysts for α-Olefin Polymerization: A ^{13}C NMR Spectroscopic Investigation. *Macromolecules* **2017**, *50*, 7010–7027. [CrossRef]
13. Gates, D.P.; Svejda, S.A.; Oňate, E.; Killian, C.M.; Johnson, L.K.; White, P.S.; Brookhart, M. Synthesis of Branched Polyethylene Using (α-Diimine)nickel(II) Catalysts: Influence of Temperature, Ethylene Pressure, and Ligand Structure on Polymer Properties. *Macromolecules* **2000**, *33*, 2320–2334. [CrossRef]
14. Wegner, M.M.; Ott, A.K.; Rieger, B. Gas Phase Polymerization of Ethylene with Supported α-Diimine Nickel(II) Catalysts. *Macromolecules* **2010**, *43*, 3624–3633. [CrossRef]
15. Camacho, D.H.; Salo, E.V.; Ziller, J.W.; Guan, Z. Cyclophane-Based Highly Active Late-Transition-Metal Catalysts for Ethylene Polymerization. *Angew. Chem. Int. Ed.* **2004**, *43*, 1821–1825. [CrossRef] [PubMed]
16. Gao, H.; Hu, H.; Zhu, F.; Wu, Q. A thermally robust amine–imine nickel catalyst precursor for living polymerization of ethylene above room temperature. *Chem. Commun.* **2012**, *48*, 3312–3314. [CrossRef] [PubMed]
17. Li, L.; Jeon, M.; Kim, S.Y. Synthesis, characterization and ethylene polymerisation of 9,10-phenanthrenequinone-based nickel(II)-α-diimine complexes. *J. Mol. Catal. A Chem.* **2009**, *303*, 110–116. [CrossRef]
18. Carlini, C.; Macinai, A.; Masi, F.; Galletti, A.M.R.; Santi, R.; Sbrana, G.; Sommazzi, A. Ethylene Polymerization by Bis(salicylaldiminate)nickel(II)/Aluminoxane Catalysts. *J. Polym. Sci. Part A Polym. Chem.* **2004**, *42*, 2534–2542. [CrossRef]
19. Popeney, C.S.; Guan, Z. Ligand Electronic Effects on Late Transition Metal Polymerization Catalysts. *Organometallics* **2005**, *24*, 1145–1155. [CrossRef]
20. Popeney, C.S.; Guan, Z. Effect of Ligand Electronics on the Stability and Chain Transfer Rates of Substituted Pd(II) α-Diimine Catalysts. *Macromolecules* **2010**, *43*, 4091–4097. [CrossRef]
21. Lanza, G.; Fragala, I.L.; Marks, T.J. Ligand Substituent, Anion, and Solvation Effects on Ion Pair Structure, Thermodynamic Stability, and Structural Mobility in "Constrained Geometry" Olefin Polymerization Catalysts: An Ab Initio Quantum Chemical Investigation. *J. Am. Chem. Soc.* **2000**, *122*, 12764–12777. [CrossRef]
22. Saeed, H.; Mahmood, Q.; Yuan, R.; Wang, Y.; Zou, S.; Tahir, K.F.; Ma, Y.; Liang, T.; Sun, W.-H. High-performance polyethylene elastomers using a hybrid steric approach in α-diimine nickel precatalysts. *Polym. Chem.* **2024**, *15*, 1437–1452. [CrossRef]
23. Kuhn, P.; S-emeril, D.; Jeunesse, C.; Matt, D.; Neuburger, M.; Mota, A. Ethylene Oligomerisation and Polymerisation with Nickel Phosphanylenolates Bearing Electron-Withdrawing Substituents: Structure–Reactivity Relationships. *Chem. Eur. J.* **2006**, *12*, 5210–5219. [CrossRef]
24. Hu, Z.; Ren, G.; Mahmood, Q.; Yu, Z.; Wang, Y.; Tahir, K.F.; Zou, S.; Liang, T.; Sun, W.-H. Thermostability promotion of α-diimine nickel precatalysts tailored with 2,6-bis(bis(4-fluorophenyl)methyl)-3,4,5-trimethoxyaniline for PE elastomer synthesis. *New J. Chem.* **2024**, *48*, 12174–12187. [CrossRef]

25. Sun, W.-H.; Jie, S.; Zhang, S.; Zhang, W.; Song, Y.; Ma, H.; Chen, J.; Wedeking, K.; Fröhlich, R. Iron Complexes Bearing 2-Imino-1,10-phenanthrolinyl Ligands as Highly Active Catalysts for Ethylene Oligomerization. *Organometallics* **2006**, *25*, 666–677. [CrossRef]
26. Ittel, S.D.; Johnson, L.K.; Brookhart, M. Late-Metal Catalysts for Ethylene Homo- and Copolymerization. *Chem. Rev.* **2000**, *100*, 1169–1203. [CrossRef]
27. Bianchini, C.; Giambastiani, G.; Luconi, L.; Meli, A. Olefin oligomerization, homopolymerization and copolymerization by late transition metals supported by (imino)pyridine ligands. *Coord. Chem. Rev.* **2010**, *254*, 431–455. [CrossRef]
28. Wang, Z.; Liu, Q.; Solan, G.A.; Sun, W.-H. Recent advances in Ni-mediated ethylene chain growth: N_{imine}-donor ligand effects on catalytic activity, thermal stability and oligo-/polymer structure. *Coord. Chem. Rev.* **2017**, *350*, 68–83. [CrossRef]
29. Mahmood, Q.; Hu, Z.; Ren, G.; Sun, W.-H. Recent Advances in Nickel Catalysis for Thermoplastic Polyethylene Elastomers: Synthesis Strategies, Properties, and Future Perspectives. *Coord Chem. Rev.* **2025**, *541*, 216833. [CrossRef]
30. Suo, H.; Solan, G.A.; Ma, Y.; Sun, W.-H. Developments in compartmentalized bimetallic transition metal ethylene polymerization catalysts. *Coord. Chem. Rev.* **2018**, *372*, 101–116. [CrossRef]
31. Mahmood, Q.; Sun, W.-H. *N*,*N*-chelated nickel catalysts for highly branched polyolefin elastomers: A survey. *R. Soc. Open Sci.* **2018**, *5*, 180367. [CrossRef]
32. Mahmood, Q.; Sun, W.-H. *Late Transition Metal Catalysts (Ni and Pd) for Ethylene Polymerization, Chapter in Encyclopedia of Polymers, Polymeric Materials, and Polymer Technology*; Mishra, M.K., Takeuchi, D., Sudo, A., Eds.; CRC Press: Boca Raton, FL, USA, 2025. [CrossRef]
33. Wang, Y.; Gao, R.; Gou, Q.; Lai, J.; Zhang, R.; Li, X.; Guo, Z. Developments in late transition metal catalysts with high thermal stability for ethylene polymerization: A crucial aspect from laboratory to industrialization. *Eur. Polym. J.* **2022**, *181*, 111693. [CrossRef]
34. Rhinehart, J.L.; Brown, L.A.; Long, B.K. A Robust Ni(II) α-Diimine Catalyst for High Temperature Ethylene Polymerization. *J. Am. Chem. Soc.* **2013**, *135*, 16316–16319. [CrossRef]
35. Wu, R.; Wang, Y.; Zhang, R.; Guo, C.-Y.; Flisak, Z.; Sun, Y.; Sun, W.-H. Finely tuned nickel complexes as highly active catalysts affording branched polyethylene of high molecular weight: 1-(2,6-Dibenzhydryl-4-methoxyphenylimino)-2-(arylimino)acenaphthylenenickel halides. *Polymer* **2018**, *153*, 574–586. [CrossRef]
36. Kong, S.; Guo, C.-Y.; Yang, W.; Wang, L.; Sun, W.-H.; Glaser, R. 2,6-Dibenzhydryl-N-(2-phenyliminoacenaphthylenylidene)-4-chloroaniline nickel dihalides: Synthesis, characterization and ethylene polymerization for polyethylenes with high molecular weights. *J. Organomet. Chem.* **2013**, *725*, 37–45. [CrossRef]
37. Fan, L.; Du, S.; Guo, C.-Y.; Hao, X.; Sun, W.-H. 1-(2,6-Dibenzhydryl-4-fluorophenylimino)-2-aryliminoacenaphthylylnickel Halides Highly Polymerizing Ethylene for the Polyethylenes with High Branches and Molecular Weights. *J. Polym. Sci. Part A Polym. Chem.* **2015**, *53*, 1369–1378. [CrossRef]
38. Mahmood, Q.; Zeng, Y.; Wang, X.; Sun, Y.; Sun, W.-H. Advancing polyethylene properties by incorporating NO_2 moiety in 1,2-bis(arylimino)acenaphthylnickel precatalysts: Synthesis, characterization and ethylene polymerization. *Dalton Trans.* **2017**, *46*, 6934–6947. [CrossRef]
39. Liu, M.; Zhang, R.; Ma, Y.; Han, M.; Solan, G.A.; Yang, W.; Liang, T.; Sun, W.-H. Trifluoromethoxy-substituted nickel catalysts for producing highly branched polyethylenes: Impact of solvent, activator and *N*,*N*′-ligand on polymer properties. *Polym. Chem.* **2022**, *13*, 1040–1058. [CrossRef]
40. Du, S.; Kong, S.; Shi, Q.; Mao, J.; Guo, C.; Yi, J.; Liang, T.; Sun, W.-H. Enhancing the Activity and Thermal Stability of Nickel Complex Precatalysts Using 1-[2,6-Bis(bis(4-fluorophenyl)methyl)-4-methylphenylimino]-2-aryliminoacenaphthylene Derivatives. *Organometallics* **2015**, *34*, 582–590. [CrossRef]
41. Zhang, Q.; Zhang, R.; Ma, Y.; Solan, G.A.; Liang, T.; Sun, W.-H. Branched polyethylenes attainable using thermally enhanced bis(imino)acenaphthene-nickel catalysts: Exploring the effects of temperature and pressure. *Appl. Catal. A* **2019**, *573*, 73–86. [CrossRef]
42. Wu, R.; Wang, Y.; Guo, L.; Guo, C.-Y.; Liang, T.; Sun, W.-H. Highly Branched and High-Molecular-Weight Polyethylenes Produced by 1-[2,6-Bis(bis(4-fluorophenyl)methyl)-4-$MeOC_6H_2N$]-2-aryliminoacenaphthylnickel(II) halides. *J. Polym. Sci. Part A Polym. Chem.* **2019**, *57*, 130–145. [CrossRef]
43. Wang, Y.; Vignesh, A.; Qu, M.; Wang, Z.; Sun, Y.; Sun, W.-H. Access to polyethylene elastomers via ethylene homo-polymerization using *N*,*N*′-nickel(II) catalysts appended with electron withdrawing difluorobenzhydryl group. *Eur. Polym. J.* **2019**, *117*, 254–271. [CrossRef]
44. Wang, X.; Fan, L.; Yuan, Y.; Du, S.; Sun, Y.; Solan, G.A.; Guo, C.Y.; Sun, W.-H. Raising the *N*-aryl fluoride content in unsymmetrical diaryliminoacenaphthylenes as a route to highly active nickel(II) catalysts in ethylene polymerization. *Dalton Trans.* **2016**, *45*, 18313–18323. [CrossRef]

45. Zhang, R.; Wang, Z.; Ma, Y.; Solan, G.A.; Sun, Y.; Sun, W.-H. Plastomeric-like polyethylenes achievable using thermally robust *N*,*N*′-nickel catalysts appended with electron withdrawing difluorobenzhydryl and nitro groups. *Dalton Trans.* **2019**, *48*, 1878–1891. [CrossRef] [PubMed]
46. Leroux, F.R.; Manteau, B.; Vors, J.-P.; Pazenok, S. Trifluoromethyl ethers–synthesis and properties of an unusual substituent. *Beilstein J. Org. Chem.* **2008**, *4*, 13. [CrossRef] [PubMed]
47. Wang, L.; Liu, M.; Mahmood, Q.; Yuan, S.; Li, X.; Qin, L.; Zou, S.; Liang, T.; Sun, W.-H. Enhancing the Thermal Stability of α-Diimine Ni(II) Catalysts for ethylene polymerization via Symmetrical axial shielding strategy. *Eur. Polym. J.* **2023**, *194*, 112112. [CrossRef]
48. Hosseinzadeh, Z.; Liu, M.; Zhang, Q.; Liang, T.; Solan, G.A.; Ma, Y.; Sun, W.-H. Electronic Tuning of Sterically Encumbered 2-(Arylimino)Pyridine-Nickel Ethylene Polymerization Catalysts by Para-Group Modification. *Catalysts* **2022**, *12*, 1520. [CrossRef]
49. Wang, R.; Sui, X.; Pang, W.; Chen, C. Ethylene Polymerization by Xanthene-Bridged Dinuclear α-Diimine Ni^{II} Complexes. *ChemCatChem* **2016**, *8*, 434–440. [CrossRef]
50. Zhang, Y.; Zhang, Y.; Hu, X.; Wang, C.; Jian, Z. Advances on Controlled Chain Walking and Suppression of Chain Transfer in Catalytic Olefin Polymerization. *ACS Catal.* **2022**, *12*, 14304–14320. [CrossRef]
51. Svejda, S.A.; Brookhart, M. Ethylene Oligomerization and Propylene Dimerization Using Cationic (α-Diimine)nickel(II) Catalysts. *Organometallics* **1999**, *18*, 65–74. [CrossRef]
52. HelldÖrfer, M.; Milius, W.; Alt, H.G. The influence of the ligand structure on the properties of (α-diimine)nickel catalysts in the polymerization and oligomerization of ethylene. *Inorg. Chim. Acta* **2003**, *351*, 34–42. [CrossRef]
53. Bahuleyan, B.K.; Son, G.W.; Park, D.-W.; Ha, C.-S.; Kim, I. Ethylene Polymerization by Sterically and Electronically Modulated Ni(II) a-Diimine Complexes. *J. Polym. Sci. Part A Polym. Chem.* **2008**, *46*, 1066–1082. [CrossRef]
54. Ye, Z.B.; Xu, L.X.; Dong, Z.M.; Xiang, P. Designing polyethylenes of complex chain architectures *via* Pd–diimine-catalyzed "living" ethylene polymerization. *Chem. Commun.* **2013**, *49*, 6235–6255. [CrossRef]
55. Britovsek, G.J.P.; Cohen, S.A.; Gibson, V.C.; Meurs, M.V. Iron Catalyzed Polyethylene Chain Growth on Zinc: A Study of the Factors Delineating Chain Transfer versus Catalyzed Chain Growth in Zinc and Related Metal Alkyl Systems. *J. Am. Chem. Soc.* **2004**, *126*, 10701–10712. [CrossRef] [PubMed]
56. Hu, X.; Zhang, Y.; Li, B.; Jian, Z. Fluorinated α-Diimine Nickel Mediated Ethylene(Co)Polymerization. *Chem.-A Eur. J.* **2021**, *27*, 11935–11942. [CrossRef] [PubMed]
57. Li, S.; Dai, S. 8-Arylnaphthyl substituent retarding chain transfer in insertion polymerization with unsymmetrical α-diimine systems. *Polym. Chem.* **2020**, *11*, 7199–7206. [CrossRef]
58. Galland, G.B.; de Souza, R.F.; Mauler, R.S.; Nunes, F.F. ^{13}C NMR determination of the composition of linear low-density polyethylene obtained with [η^3-methallyl-nickel-diimine]PF_6 complex. *Macromolecules* **1999**, *32*, 1620–1625. [CrossRef]
59. Dolomanov, O.V.; Bourhis, L.J.; Gildea, R.J.; Howard, J.A.K.; Puschmann, H. OLEX2: A complete structure solution, refinement and analysis program. *J. Appl. Cryst.* **2009**, *42*, 339–341. [CrossRef]
60. Sheldrick, G.M. SHELXT—Integrated space-group and crystalstructure determination. *Acta Cryst.* **2015**, *A71*, 3–8.
61. Sheldrick, G.M. Crystal structure refinement with SHELXL. *Acta Cryst.* **2015**, *C71*, 3–8.

Disclaimer/Publisher's Note: The statements, opinions and data contained in all publications are solely those of the individual author(s) and contributor(s) and not of MDPI and/or the editor(s). MDPI and/or the editor(s) disclaim responsibility for any injury to people or property resulting from any ideas, methods, instructions or products referred to in the content.